



Review

Review of Desert Mobility Assessment and Desertification Monitoring Based on Remote Sensing

Zhaobin Wang ^{1,*} , Yue Shi ¹ and Yaonan Zhang ²

¹ School of Information Science and Engineering, Lanzhou University, Lanzhou 730000, China; shiyue@lzu.edu.cn

² The National Cryosphere Desert Data Center, Northwest Institute of Eco-Environment and Resources, Chinese Academy of Sciences, Lanzhou 730000, China; yaonan@lzb.ac.cn

* Correspondence: wangzhh@lzu.edu.cn; Tel.: +86-931-8912778

Abstract: Desertification seriously hinders economic development and ecological security, which has led to increased research on desertification monitoring and control. Remote sensing technology is widely used in desert research due to its large detection range and ability to obtain target feature information without touching objects. In order to better monitor and control desertification, the research methods on desert mobility and dune morphology in mobile deserts were reviewed. Among them, an important index to distinguish mobile and nonmobile deserts is desert vegetation coverage. The research progress of desert vegetation coverage based on visual interpretation, the nonlinear spectral model, normalized vegetation index (NDVI) fitting and plant community classification was reviewed. The loss of vegetation in the transitional zone of the desert is a contributing factor to desertification. The new technologies and applications of desert area monitoring, the remote sensing ecological index, and desert feature information extraction were introduced and analyzed. To combat desertification more accurately and effectively, the classification methods of moving dunes based on deep learning were also reviewed. It can be concluded that desertification monitoring methods are gradually becoming more accurate and adaptive, but they remain insufficient and less mature. Therefore, exploring how to apply desertification control technology more scientifically and rationally is an extremely valuable area for research.

Keywords: desert mobility; desertification monitoring; classification of dune types; deep learning; remote sensing image



Citation: Wang, Z.; Shi, Y.; Zhang, Y. Review of Desert Mobility

Assessment and Desertification

Monitoring Based on Remote

Sensing. *Remote Sens.* **2023**, *15*, 4412.

<https://doi.org/10.3390/rs15184412>

Academic Editor: Pavel Kishcha

Received: 3 June 2023

Revised: 1 August 2023

Accepted: 13 August 2023

Published: 7 September 2023



Copyright: © 2023 by the authors. Licensee MDPI, Basel, Switzerland. This article is an open access article distributed under the terms and conditions of the Creative Commons Attribution (CC BY) license (<https://creativecommons.org/licenses/by/4.0/>).

1. Introduction

Desertification monitoring and research on desert mobility have emerged as crucial topics in contemporary society, as they have increasingly significant implications for social development and human survival. In recent years, the delicate balance of natural ecosystems has been disrupted due to the combined influence of human activities and natural factors. Drought and wind are the two primary causes of desert formation, while deforestation leads to the loss of vegetation cover and the degradation of grasslands [1]. The consequences of desertification pose severe threats to regional biodiversity and the sustainable development of human populations. The associated socioeconomic and ecological challenges have become pervasive worldwide, thus capturing the attention of nations across the globe. As sustainable development becomes increasingly imperative, the accurate and efficient classification of mobile desert areas becomes paramount. This classification serves as a foundation for monitoring desert mobility, thereby aiding in the resolution of the deteriorating desertification problem. This review aims to consolidate the current research status in the academic field by focusing on desert remote sensing information within the broader context of desert scientific research. By examining the advancements in this field, we can gain insights into the effective monitoring techniques and strategies for addressing the challenges posed by desertification.

Approximately one-quarter of the Earth's land area is affected by desertification, and the global extent of desertification is still expanding. Over 20% of the world's arable land, 30% of forests, and 10% of grasslands are experiencing degradation [2]. China, in particular, features the world's largest desert region and is one of the countries most severely affected by desertification [3]. Additionally, desertified land is found in various pockets throughout the country, with the country consequently experiencing severe impacts from desertification. Given the context of global warming and increasing aridity, the activation of sand dunes and the expansion of deserts have intensified. Consequently, the task of protecting and consolidating these regions remains challenging and demanding [4].

Currently, the research on deserts utilizing remote sensing images combined with deep-learning techniques has yielded a wealth of valuable insights. However, there is a need for a more comprehensive integration of these approaches. To address this, we have conducted a thorough summary and comparative analysis. The specific structural framework is shown in Figure 1. Prior to conducting research, it was necessary to select a desert remote sensing dataset and perform data preprocessing. After completing these preliminary tasks, due to the occurrence of desertification in mobile deserts, it was first necessary to monitor and classify mobile and nonmobile deserts, followed by monitoring the desertification within mobile deserts. Finally, in order to obtain a more accurate understanding of desertification conditions, the further classification and monitoring of the morphological types of mobile deserts were carried out. This review compares and summarizes the research methods in these areas, thus aiming to provide an overview of the current research status and explore future research directions.

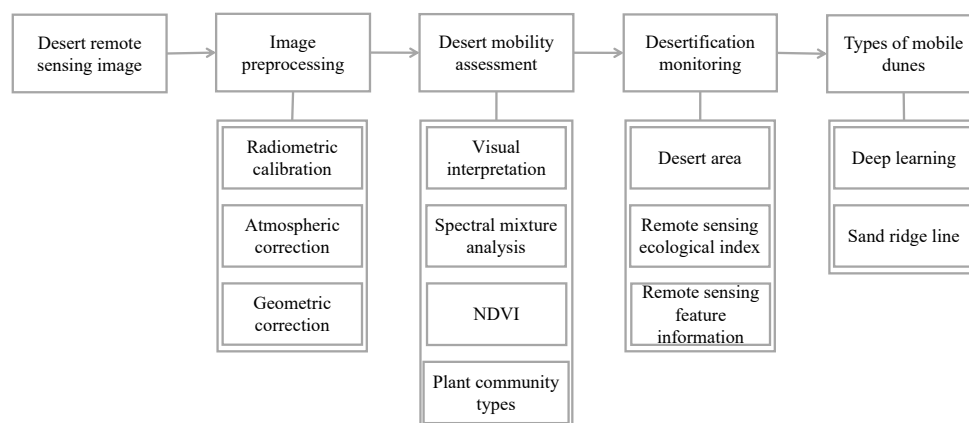


Figure 1. Framework of desertification monitoring.

In the realm of remote sensing information for desert research, various types of remote sensing data are employed, with each possessing distinct observation ranges that are attributed to their varying resolutions. The availability of diverse and extensive desert remote sensing datasets serves as a dependable foundation, thus providing a reliable assurance for conducting desert research. Nevertheless, it is crucial to acknowledge the indispensability of the preprocessing step when utilizing remote sensing datasets for desert research. The preprocessing steps include radiometric calibration, as well as atmospheric and geometric correction, so as to optimize the data set, remove the noise in the image, avoid the spectral brightness distortion, and reduce the experimental error [5]. The purpose of radiometric calibration is to eliminate the error of the sensor itself and to determine the accurate radiation value at the entrance of the sensor. The purpose of atmospheric correction is to eliminate the error caused by atmospheric scattering, absorption, and reflection. The purpose of geometric correction is to eliminate the geometric distortion caused by atmospheric transmission, the sensor itself, the Earth's curvature, and other factors. The successful preparation of dataset preprocessing is the basis of desertification monitoring and desert mobility research.

The monitoring of desertification is firstly based on the classification of mobile deserts, and the index to distinguish mobile deserts from nonmobile deserts is vegetation coverage [6]. Zhang et al. [7] realized the visual interpretation of desert vegetation by establishing interpretation markers. While the visual interpretation method is subjective and has low accuracy, spectral hybrid analysis can further accurately invert vegetation coverage. At the same time, plant community differentiation is conducive to desertification control through its potential interactions [8,9]. The monitoring methods for desert vegetation coverage in this review were mainly compared and analyzed, including visual interpretation, spectral mixture analysis, vegetation estimation models, and plant community differentiation. Because of their mobility, mobile deserts have the problem of expanding or intensifying desertification. Early studies were limited to monitoring desert areas. Firstly, the basic types of deserts and grasslands in the desert were extracted to monitor the area change. Pi et al. [10] proposed the desert grassland classification network (DGC) and used three-dimensional convolutional neural network (3D-CNN) models to identify deserts and grasslands. Moghaddam et al. [11] used multilayer perceptron (MLP) to classify desert images. The ecological quality in deserts can be assessed by the RSEI. Xu [12] proposed the RSEI through principal component coupling greenness, dryness, humidity, and heat, and the author took the first principal component as the RSEI value. The further development of RSEI has made desertification monitoring more concrete. In order to obtain the desert information, researchers have carried out the research of extracting the desert feature information. The desert can be classified quickly and accurately from remote sensing images. Therefore, from the monitoring of desert area change, the desert remote sensing ecological index (RSEI), and the acquisition of desert feature information, the research and comparative analysis have been carried out so as to achieve desertification control. In order to further understand the structure of the desert and to grasp the trend of the desert, many researchers have carried out studies on the morphology and types of deserts [13]. Zhao et al. [14] firstly divided the Chinese desert (sandy land) into fixed dunes, semifixed dunes, and mobile dunes according to the classification method of mobility and then subdivided the categories into barchan dunes and dune chains according to the morphological method. Li et al. [15] divided the north bank of the Luanhe River in China into horizontal dunes, barchan dunes, star dunes, and flat sandy land. However, this classification is mainly limited to the morphology of the dune. This review further conducted comparative analysis of the research on sand dune morphology, as well as the extraction and classification of sand ridge lines.

Hence, the study of desertification holds immense significance. However, despite the advances in estimating vegetation coverage through linear spectral mixing models, which have made some progress in the context of desert flow monitoring, there still exist issues with inaccurate estimation. Furthermore, there is a need to enhance the accuracy and stability of remote sensing estimation models. Challenges remain in the monitoring of desert areas and the classification of desert types, as misclassification issues persist, and the available characteristic information remains limited. In the evaluation of desert ecological environment quality, the utilization of remote sensing ecological indices aims to explore more efficient index combinations and algorithms. Additionally, the extraction of dune types and sand ridge lines calls for the development of more lightweight and high-precision networks to ensure improved accuracy.

2. Desert Remote Sensing Image Preprocessing

Preprocessing serves as the crucial initial step in remote sensing applications, and the current technology in this domain has reached a high level of maturity. While the raw dataset may contain unprocessed information, image preprocessing is necessary to eliminate irrelevant image data and restore meaningful and actionable image data. This process enables the detection of more relevant information within the images, thereby consequently reducing the overall data requirements. By enhancing the reliability of feature extraction,

image segmentation, matching, and recognition, the quality and accuracy of the subsequent analysis can be improved.

2.1. Dataset Status

To facilitate desertification monitoring and desert mobility research, the availability of suitable desert remote sensing datasets is paramount. Currently, a variety of datasets are utilized for research involving desert remote sensing images. Table 1 provides a summary of the commonly used remote sensing datasets in desert research. These datasets play a crucial role in providing the necessary data foundation for conducting comprehensive analyses and investigations in the field of desert research.

Table 1. Satellite datasets details.

Satellite Dataset	Nation	Spatial Resolution (m)	Launch Time	Characteristics
ALOS1	Japan	2.5/10/100	2006	Facilitates convenient stereo mapping; large-scale coarse-resolution data; and small-scale fine-resolution data.
ALOS2	Japan	1/10/100	2014	High-speed and large-capacity data processing; precise satellite positioning and attitude control.
SPOT5	France	2.5/10	2002	Front-to-back mode; good performance in data compression, storage, and transmission.
SPOT6	France	1.5/6	2012	High resolution.
SPOT7	France	1.5/6	2014	Includes a variety of imaging modes, including long strips, large areas, multipoint targets, dual-image stereo, and triple-image stereo, etc.
MODIS	America	250/500/1000	1999	It is the only onboard instrument on the satellite that broadcasts to feature real-time observation data directly to the world through the X-band.
Gaofen1	China	2/8/16	2013	High spatial resolution; multispectral; wide coverage.
Gaofen2	China	0.8/3.2	2014	Submeter spatial resolution; high positioning accuracy; fast attitude maneuverability.
Gaofen6	China	2/8/16	2018	The time resolution of remote sensing data acquisition is shortened from 4 days to 2 days.
Landsat7	America	15/30/60	1999	“The most stable and best-performing Earth observation instrument ever built.”
Landsat8	America	15/30/100	2013	Long time in orbit; many bands
Landsat9	America	15/30/100	2021	Greater radiometric precision; slightly improves the overall signal-to-noise ratio.
Sentinel2	European Space Agency	10/20/60	2015	It is primarily used for global high-resolution and high-revisit capability land observation; features mapping of biophysical changes, monitoring coastal zones, and inland water bodies, as well as disaster mapping.
World-View3	America	0.31/1.24	2014	Multiple payloads; hyperspectral; high resolution.
NOAA	America	1.1	1994	Its main application is in large-scale regions.

The SPOT series of satellites, which was developed by the French Centre for Space Research (CNES), serves as an Earth observation satellite system. The satellites offer varying spatial resolutions of 5 m, 10 m, and 20 m. On the other hand, the ALOS satellite is Japan’s prominent earth observation satellite, which features advanced capabilities such as high-speed and large-capacity data processing technology, as well as precise satellite positioning and attitude control technology. Zhang et al. [7] used ALOS and SPOT5 high-resolution remote sensing images, combined with field investigations, to complete the visual interpretation of the remote sensing image information and vegetation mapping of the Ulan Buhe Desert research area in Inner Mongolia, China. Based on the long-term SPOT–vegetation remote sensing data, Kuang et al. [16] analyzed the intensity and trends of land degradation in Central Asia from 1999 to 2012 by combining the Theil [17,18], slope estimation, and Ma [19–25] trend tests. The ALOS and SPOT datasets offer relatively high spatial resolution, which proves advantageous for extracting desert vegetation and monitoring the extent of

land degradation. It contributes to the overall quality and utility of the ALOS and SPOT datasets in supporting desert vegetation analysis and land degradation monitoring.

MODIS, which is an essential sensor aboard the TERRA and AQUA satellites, assumes a significant role in Earth observation. Liu et al. [26] used long-time series MODIS–NDVI data to construct a vegetation coverage inversion model in desert areas, and they studied their spatial distributions, dynamic changes, and development trends. The long-term characteristics of MODIS data provide a scientific basis for sand control, vegetation restoration, and ecological construction in the fragile ecological zone on the edge of the Badain Jaran Desert.

In 2014, the Gaofen-2 (GF-2) satellite was successfully launched, thus marking a significant milestone for China, as it became the first country to develop a self-engineered civilian optical remote sensing satellite with a spatial resolution greater than 1m. This accomplishment signifies the advent of the “Gaofen era” for China’s remote sensing satellites, thus ushering in a new era of submicron capabilities. Yue et al. [27] used the GF-2 remote sensing images to register the aerial images with them, and they calculated the vegetation coverage of the aerial images by using the NDVI cells of the satellite images as the statistical unit. The empirical relationship between the two was established using fitting data, and then the vegetation coverage estimation model was obtained using remote sensing. Sun et al. [28] processed the images using the multiple endmember spectral mixture analysis of the 16-period Gaofen-1, and they then performed a cross-wavelet transform (XWT) to extract feedback features as the feature parameters. The high resolution of the high-resolution satellite dataset makes it widely used in desert feature extraction.

Following its launch in 1999, Landsat 7 emerged with sensors that were renowned for their exceptional stability and performance, thereby solidifying its position as a premier Earth observation instrument. Subsequently, Landsat 8 commenced image acquisition after a successful 100-day test run starting in 2013. Most recently, in 2021, Landsat 9 achieved a successful launch from the Vandenberg Space Force Base in California. Chang et al. [29] used Landsat 7 ETM and L1T remote sensing images of the Tengger Desert in 2000 and 2002, which constituted a total of eight scenes. Based on the Landsat 8 images, Liu [30] studied the extraction algorithms of desert areas, which has practical significance for the effective monitoring of desert areas. Melichar et al. [31] used the multitemporal Landsat8 Operational Land Imager spectral images from the period of 2013–2020 to prototype a novel approach to desert vegetation classification using RF machine-learning methods. Within the realm of desert research, numerous scholars have extensively utilized Landsat data owing to its favorable attributes, including a short imaging cycle, convenient data acquisition, a high signal-to-noise ratio of images, and a notable spatial resolution. Consequently, it has garnered considerable attention from the scientific community. The recent addition of Landsat 9 further enhanced the field of study by capturing Earth’s surface observations with a heightened radiometric precision and a slight improvement in the overall signal-to-noise ratio. As a result, Landsat 9 presents a more accurate and reliable dataset, thereby paving the way for future research endeavors in the field of desert studies.

Moreover, Sentinel-2 serves as a valuable complement to other satellite missions, such as Landsat, thereby enhancing the overall capabilities of Earth observation endeavors. The utilization of Sentinel-2 imagery in desert research facilitates a comprehensive understanding of desert ecosystems and supports various applications in this field. Since the launch of Sentinel-2 multispectral instruments in 2015, there have been many studies on land cover/use classification that have used Sentinel-2 images [32]. Chen et al. [33] combined Landsat-8 and Sentinel-2 datasets with the RF model, and they selected the crust index(CI) and biological soil crust index(BSCI) to detect the biological soil crusts (BSCs) coverage in the Mu Us Desert in northern China. Ali et al. [34] employed optical image matching and a singular value decomposition approach to estimate the rates of dune migration in the North Sinai Sand Sea using the free Landsat 8 and Sentinel-2 archives. Al-Ali et al. [35] used Sentinel-2A remote sensing images to detect the temporal and spatial changes of vegetation coverage from 2017 to 2020. While Sentinel-2 presents numerous

opportunities for land cover and land use classification, it is essential to address certain challenges that arise in its application. These challenges encompass issues such as potential mismatches with Landsat OLI-8 data, the absence of thermal bands, and variances in the spatial resolutions among the bands of Sentinel-2. Despite these challenges, Sentinel-2 data exhibit considerable promise and hold the potential to make substantial contributions to the field of land cover and land use monitoring. Further research and methodological advancements can harness the strengths of Sentinel-2 data, thereby enabling their effective utilization in land cover and land use analysis.

Sand dunes are inherently dynamic and susceptible to alterations in their locations, shapes, and dimensions due to environmental factors. To effectively monitor sand dune movement, the utilization of multitemporal satellite images has become a common practice. Els [36] compared coarse (Landsat)- and fine (Worldview)-resolution images. For the study of dune morphology and movement in sand sea, Landsat was sufficient. With the deepening of the research, the requirements for resolution have become higher. At this time, a satellite known as Worldview has been introduced. It allows researchers to obtain more detailed information, and it can better carry out research on the specific dynamics of specific dunes, as well as climate and environmental changes in the time dimension. Guo et al. [37] used the NOAA satellite AVHRR data to study the process of multiple sandstorms from 2000 to 2002, and they analyzed the spectral characteristics of different targets such as sand, cloud, desert, Gobi, snow, bare ground, and vegetation. Sandstorms have been reflected in AVHR-2 channels to varying degrees, and the dust information can be effectively extracted by using the multichannel combined dust index.

These images provide valuable insights into the temporal dynamics of sand dunes. Additionally, there exist numerous remote sensing satellites that are well-suited for conducting research on dunes. These satellites offer valuable data and resources for studying the intricate processes and changes associated with sand dunes. Their utilization enhances our understanding of dune dynamics and facilitates the comprehensive monitoring and analysis of these natural formations.

2.2. Status of Preprocessing

To enhance the effectiveness of data mining, it is crucial to preprocess the datasets beforehand. Remote sensing data preprocessing involves several key steps, including radiometric calibration, atmospheric correction, geometric correction, image mosaicking, cropping, cloud and shadow removal, and spectral normalization. In this paper, we primarily focused on the initial three sections, namely, radiometric calibration, atmospheric correction, and geometric correction, which play a significant role in ensuring the quality and accuracy of the data for subsequent analysis and interpretation. Figures 2 and 3 illustrate the data preprocessing for the Landsat 8 and GF-1 datasets, respectively, for complete coverage of the Tengger Desert region in 2022.

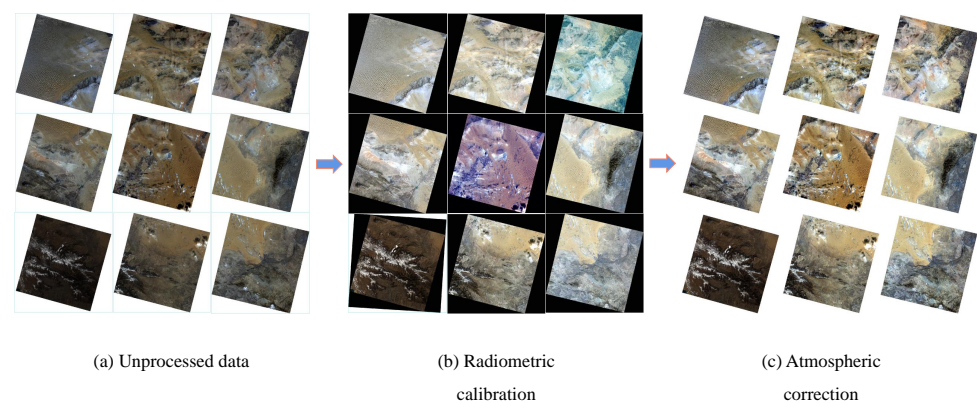


Figure 2. Data preprocessing of Landsat8 dataset in Tengger Desert region in 2022.

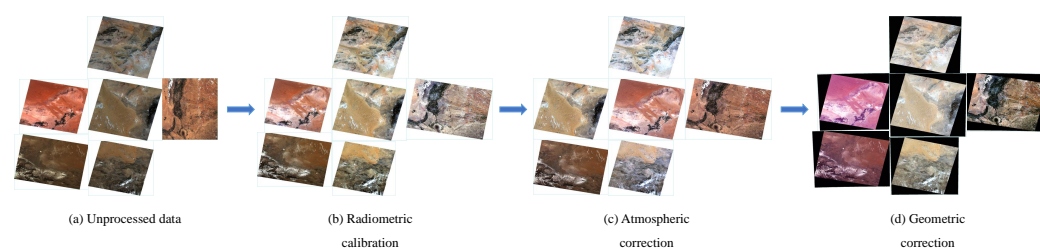


Figure 3. Data preprocessing of GF-1 dataset in Tengger Desert region in 2022.

2.2.1. Radiometric Calibration

When determining the spectral reflectance or spectral radiance of ground objects, it is crucial to convert the brightness grayscale values of the multispectral image into absolute radiance values. Han et al. [38] proposed a new radiometric cross-calibration method for the wide field of view. It could obtain reliable radiometric cross-calibration results for each band, even without the available corresponding reference bands. Tang et al. [39] performed calibration based on grayscale permanent artificial targets and multiple radiometric calibration tarpaulins (tarps) using a reflectance-based approach. Tang et al. [40] then proposed an irradiance-based absolute radiometric calibration campaign. The results suggested that the irradiance-based method was better than the reflectance-based method. Additionally, apart from atmospheric radiation interference, the remote sensors' radiation information of ground objects may contain systematic errors, such as recording noise and detector errors, which can distort the spectral brightness. To obtain accurate radiation information, establishing a quantitative conversion relationship between the output value of the remote sensor and the incident radiance value through radiometric calibration is essential. Various methods, including reflectance, radiance, and irradiance methods, can be employed for this purpose. The reflectance can be calculated using the method of analytical approximation, which significantly reduces computation time and complexity.

We conducted preprocessing experiments on the Landsat 8 and GF-1 datasets in Tengger, China in 2022. Figures 2a and 3a illustrate the original Landsat 8 and GF-1 datasets, respectively, thereby displaying the RGB composition. By combining different bands, various RGB schemes can be employed to interpret different features and fulfill specific requirements. To calculate the spectral reflectance or spectral radiance of the ground objects and to enable comparisons between the images captured by different sensors at different times, it was necessary to convert the grayscale values representing the image brightness into absolute radiance values. The radiometric calibration results for the two aforementioned datasets are presented in Figures 2b and 3b. The original images were radiometrically calibrated to convert the brightness grayscale values of the images to absolute radiance values. During this process, the voltage or data quantization values (DN) recorded by the sensor were converted into absolute radiance values (emissivity) or relative values associated with physical quantities, such as surface reflectance and surface temperature.

2.2.2. Atmospheric Correction

Absolute atmospheric correction methods include the MODTRAN and 6S [41,42]. The MODTRAN provides reflectivity calculations for the top atmospheric layer in bands greater than $0.2 \mu\text{m}$, while the 6S focuses on calculating the atmospheric transmission parameters within the range of $0.2 \mu\text{m}$ – $4 \mu\text{m}$. These methods typically require surface measurements of the imagery transits and the consideration of factors such as terrain relief to accurately correct for atmospheric and sensor effects. However, meeting the aforementioned conditions is often challenging for most remote sensing images available today, thus resulting in their complexity [43]. Based on the performance of the atmospheric correction processor ATCOR, Pflug et al. [44] combined two data sources and ensured the consistent quality of the atmospheric correction to obtain a denser time series. Reyes et al. [45] developed a new Python-based atmospheric correction software and outlined the underlying algorithm

of the PACO, thereby making it very easy to use for any remote sensing ground segment. Kalinskaya et al. [46] proposed an algorithm for the additional correction of satellite level 2 data that uses a two-parametric model of the Black Sea remote-sensed reflectance as a first approximation. The additional correction significantly reduced the discrepancy between in situ and retrieved remote-sensed reflectance, especially in short-wave spectral bands. By analyzing the differences in radiation values across remote sensing images captured at different time phases, change monitoring can be achieved. Relative radiation correction aims to establish consistency in the radiation values of relatively stable ground objects with identical characteristics across different time-phase remote sensing images. This enables the comprehensive monitoring of dynamic changes in ground objects using remote sensing techniques.

When conducting desert research, it is important to note that the total radiation luminance measured by the sensor does not directly reflect the true surface reflectance of the ground target. This is due to errors caused by atmospheric absorption, particularly scattering. We conducted atmospheric correction on the two datasets, and the results are illustrated in Figures 2c and 3c. The purpose of atmospheric correction is to mitigate the radiation errors introduced by atmospheric influences and retrieve the true surface reflectance of ground objects. By converting the radiance or surface reflectance values, it becomes possible to obtain the actual surface reflectance, which is valuable in mitigating atmospheric and illumination effects.

2.2.3. Geometric Correction

Geometric deformation in remote sensing images can be categorized into two types: systematic and nonsystematic. Systematic geometric deformation is caused by the sensor itself and follows regular and predictable patterns, which can be corrected using the sensor model. The original data of Landsat 8, which underwent geometric correction involving terrain data, can generally be used directly without the need for geometric correction. Figure 3d shows the geometric correction result of GF-1, which underwent orthorectification after atmospheric correction to eliminate errors caused by ground elevation. On the other hand, nonsystematic geometric deformation is irregular and can be attributed to factors such as sensor instability and changes in terrain.

Currently, there are several well-established geometric correction techniques that are suitable for processing desert remote sensing images. Co-Registration of Optically Sensed Images and Correlation (COSI Corr) is a technique used to generate the raster maps of dune movement. Baird et al. [47] were the first to apply COSI Corr to a complete Landsat archive. Hua et al. [48] proposed an automatic correction technique based on decision tree classification, which improved the correction accuracy. Wang et al. [49] developed a geometric correction algorithm based on conjugate triangles and affine transformation for remote sensing satellite data, and they then produced land-surface temperature (LST), NDVI, and aerosol products for seismic disaster monitoring. Li et al. [50] proposed an RPC coefficients optimization method based on image offset correction and positioning dominant coefficients. It could improve the geometric positioning accuracy without introducing additional compensation parameters. Their research introduced an automated workflow that was capable of automatically performing scene correlations and dune detection. Compared to previous studies, the current preprocessing methods no longer require manual operations, thus resulting in reduced labor costs and enabling faster and more intelligent research.

3. Desert Mobility Assessment

Deserts can be classified into mobile and immobile types. The characteristic of a mobile desert is its continuous migration and expansion. Consequently, the shape and position of the dunes within these deserts undergo constant changes. Mobile dunes represent one type of dunes that are classified based on their mobility and wide distribution in deserts. In contrast, nonmobile deserts emerge when vegetation covers most of the desert surface,

thereby preventing further migration and expansion. In nonmobile deserts, the shapes and locations of the dunes remain relatively stable. Numerous scholars have employed various methods to assess vegetation coverage and predict desert mobility. Based on these predictions, interventions such as artificial sand fixation and other techniques can be employed to effectively mitigate desertification in a timely manner [6,51,52].

3.1. Visual Interpretation

Visual interpretation is a fundamental skill employed in geoscience research and remote sensing applications within the information society. It serves as the most intuitive approach for studying desert vegetation coverage, thus allowing researchers to extract valuable information from desert areas through visual analysis. Visual interpretation offers the advantage of requiring minimal equipment and being simple and convenient to use, thereby enabling the acquisition of thematic information from remote sensing images at any given time.

3.1.1. Classical Methods

The Haloxylon ammodendron forest in the Ulan Buhe Desert is the largest wild Haloxylon ammodendron forest in the world [53], and it is an important ecological protection barrier in the Alxa region. For a long time, due to unreasonable human development and natural factors, the natural Haloxylon ammodendron forest has been weakened and severely damaged [54]. Due to the reduction of the Haloxylon ammodendron forest belt, its ecological functions of windbreaking and sand fixation have been seriously affected, thereby aggravating desertification. Zhang et al. [7] used the visual interpretation method of desert vegetation, mainly based on the Haloxylon ammodendron forest using remote sensing images, to establish fusion image spectral interpretation signs, as well as comprehensive analysis and interpretation signs of the vegetation habitat conditions. In order to comprehensively and systematically grasp the ecological status of Ulanbu and the desert, as well as the distribution area of the Haloxylon ammodendron forest in Ulanbu and the desert, relevant research was carried out.

After organizing and summarizing the information, the specific process of visual interpretation is illustrated in Figure 4. Once the necessary preparations for image interpretation are completed, the initial interpretation is conducted by analyzing direct features such as tone, size, shape, shadow, color, texture, and pattern, as well as indirect features such as position and relative arrangement. Based on the relationship between target features and image characteristics, an interpretation feature table of the study area is established, which serves as a reference for conducting detailed interpretation. Field verification is conducted in conjunction with the interpretation process, and the final results are visualized to enhance their understanding and presentation.

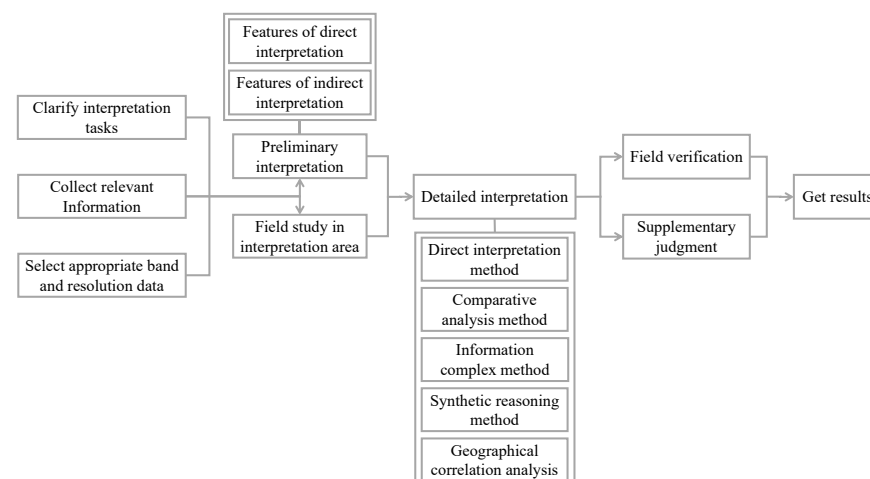


Figure 4. Visual interpretation method of desert vegetation.

3.1.2. Limitations

Visual interpretation plays a crucial role in acquiring knowledge about the types, distribution, and abundance of ground objects, thereby contributing significantly to the development and conservation of desert plant resources and the enhancement of regional ecological environments. Nevertheless, it is important to acknowledge that visual interpretation is susceptible to subjective interpretations when recognizing desert features. Furthermore, the accurate visual interpretation of desert characteristics, such as bare land, semisandy land, desert areas, and various types of dunes, necessitates the expertise and domain-specific knowledge of users.

3.2. Spectral Mixture Analysis

Desert vegetation plays a vital role in maintaining the ecological integrity of oasis ecosystems worldwide. The timely monitoring of photosynthetic and nonphotosynthetic vegetation coverage in deserts holds significant importance in guiding land desertification control practices and studying the mechanisms underlying vegetation decline. By accurately assessing and understanding the dynamics of desert vegetation, valuable insights can be gained for the effective conservation and sustainable management of these fragile ecosystems.

3.2.1. Classical Methods

The protection of desert vegetation requires a large amount of desert vegetation data [55]. Spectral mixture analysis (SMA) is a widely used and excellent method for retrieving vegetation coverage [56–58]. The method flow diagram of Figure 5 shows the process of spectral mixture analysis and validation.

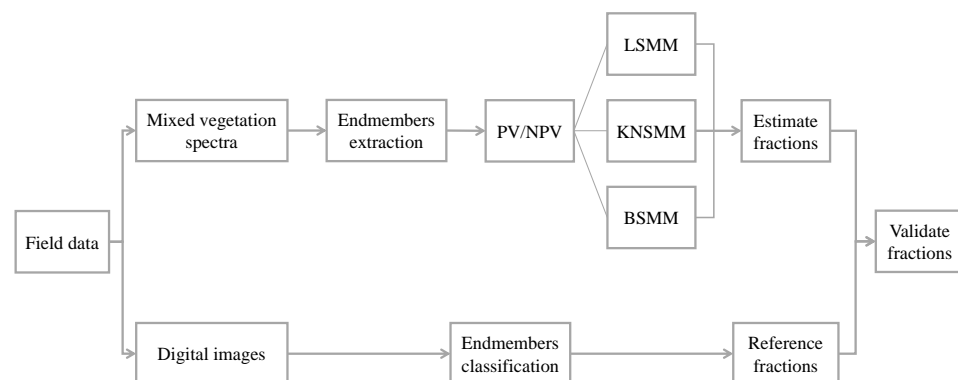


Figure 5. The process of spectral mixture analysis and validation (FCLS—fully constrained least squares; 3-EM—three-endmember models; 4-EM—four-endmember models; PV—photosynthetic vegetation; NPV—nonphotosynthetic vegetation; BS—bare soil; LSMM—linear spectral mixture model; KNSMM—kernel nonlinear spectral mixture model; BSMM—bilinear spectral mixture model).

The SMA method models the mixed spectrum into a pure spectrum through its subpixel fraction coverage weighting [59]. Ji et al. [60] constructed the LSMM based on the principles of linear mixtures [61–64]. The estimation of the PV/NPV in the desert area of Minqin County, Gansu Province, China was conducted using LSMM. Furthermore, the influence of the nonlinear spectral mixture model on the estimation of vegetation cover was investigated. The principle of the kernel nonlinear spectral mixture model (KNSMM) is that the data from the input space are mapped to the high-dimensional feature space through implicit nonlinear mapping by kernel functions. According to the characteristics of different nonlinear spectral mixture models (NSMM) [65], two relatively simple models with results of physical significance were proposed. They are the bilinear spectral mixture model (BSMM) and the kernel-based NSMM. Chen et al. [66] examined the ability of

optimized multi-endmember spectral mixture analysis (MESMA) for monitoring desert vegetation degradation, recovery, and greening in a dryland basin of Northwest China using Landsat time series data from the 1990s to 2016. Eight modeled endmember fractions were generated using the best endmember model with the lowest fraction error and root mean square error (RMSE). The abundances of nondesert vegetation, desert vegetation, soil, and impervious surface areas were incorporated based on the eight original fractions and validated using high-spatial-resolution images.

3.2.2. Limitations

The calculation process of the linear spectral mixture model (LSMM) is known for its clarity and conciseness. However, it relies on the assumption of a relatively ideal scenario without multiple scattering [67,68], which introduces certain errors and calls for further enhancements. Moreover, when it comes to nonlinear mixtures, it remains to be investigated whether different types of desert vegetation exhibit consistency. Future research should explore the applicability and limitations of the LSMM in capturing the complex spectral interactions in desert environments. The MESMA is a powerful technique for detecting desert vegetation coverage. The desert vegetation degradation, recovery, and greening can be monitored at a regional scale. The good performance indicates its potential to detect the desert vegetation changes, and it may be transferred to other arid regions. Future efforts will focus on improving the spectral resolution by fusing the images with rich spectral data and refining the validated categories to investigate the capability of the MESMA.

3.3. Fitting NDVI Data

As an evaluation index to detect vegetation growth and vegetation coverage, the NDVI has been widely used in the study of desert mobility.

3.3.1. Background

A mobile desert primarily consists of shifting sand dunes, and the formation of dunes is closely intertwined with vegetation. For instance, dense vegetation obstructs the movement of sand, thereby resulting in the accumulation of sand piles. In order to survive, plants grow taller as the sand accumulation thickens, thus contributing to the gradual growth of the sand pile. This process forms a unique sedimentary structure as the aeolian sand becomes intertwined with plant roots and litter. The vegetation provides a protective cover, but once the plants perish due to water scarcity, the sand piles become susceptible to wind erosion.

The Taklimakan Desert, known as the largest mobile desert globally, exhibits the mobility of sand dunes influenced by various factors, including moisture content, underlying topography, and vegetation conditions. When the sand dunes are moist, the sand particles become more viscous and agglomerated, thereby making them less prone to being blown and transported, which reduces the speed of dune movement. Similarly, undulating topography beneath the dunes can also impede their movement. Researchers [69,70] have classified vegetation coverage and divided it into five grades based on the normalized difference vegetation index (NDVI), as shown in Table 2. Dunes tend to move faster when vegetation coverage is low and vice versa. In areas where humidity-tolerant and wind-resistant plants hinder wind and sand movement, the mobility of dunes is extremely limited, thereby leading to the classification of such dunes as semifixed. When the ground is predominantly covered by vegetation, exceeding 30% of the total coverage, the sand movement nearly ceases, thus resulting in relatively stable dune positions. These dunes are referred to as fixed dunes. Therefore, assessing vegetation coverage through NDVI is a crucial approach for implementing plant-based sand fixation measures in desert control efforts.

Table 2. Classification of vegetation coverage.

Grading	Vegetation Coverage /%	Surface Landscape Features
Pretty-low-coverage vegetation	<10	Mainly mobile sand dunes, with sporadic vegetation coverage between the dunes, as well as water bodies, residential areas, etc.
Low-coverage vegetation	10–30	Mainly semifixed dunes; the area of quicksand is more than 50%, and the dunes are usually covered with sandy grass and shrubs.
Medium-coverage vegetation	30–50	Mainly fixed dunes and thickets of sand; the dunes are covered with lush shrubs.
Medium-to-high coverage vegetation	50–70	Sandy land with spotted quicksand distribution, as well as medium- and high-yield grassland, woodland, etc.
High-coverage vegetation	>70	High-yield woodland, swamp wetlands, etc., with lush vegetation

3.3.2. Classical Methods

The Silk Road Economic Belt traverses numerous countries, all of which face common challenges related to desertification prevention and sustainable development. Obtaining traditional vegetation coverage data through ground measurements is a time-consuming process that requires substantial effort. Consequently, the utilization of remote sensing as an indirect method for acquiring vegetation coverage data has gained prominence. Researchers have explored various estimation methods based on vegetation indices, such as empirical modeling approaches and data mining techniques such as decision tree classification [71]. This is motivated by the strong linear or nonlinear correlation observed between vegetation indices and vegetation coverage [72,73]. However, the development of remote sensing estimation models that are specifically tailored for vegetation coverage in desert areas remains limited, thereby posing significant challenges for desertification monitoring and related studies [27,74,75]. Conducting research on empirical models for the remote sensing estimation of vegetation coverage holds considerable practical significance in promoting and enhancing ecological monitoring and research in relevant regions.

Liu et al. [26] obtained high-resolution NDVI data of ground plots with a multispectral camera mounted on a UAV to calculate vegetation coverage. By studying the fitting relationship between the high-resolution satellite vegetation coverage and NDVI data, Yue et al. [27] established a linear model for the remote sensing estimation of the vegetation coverage in the northern desert of Fukang based on the NDVI derived from high-resolution satellite images. At the same time, Yue established a quadratic polynomial model for the remote sensing estimation of the desert vegetation coverage in the Karamay Plain based on the NDVI derived from ZY1-02C images. These models can provide service and reference for ecological monitoring and research in desert areas to some extent.

Fractional vegetation coverage (FVC) is a common evaluation index for desert ecosystems. In areas with less manual intervention, it has been found that the FVC can be effectively predicted by meteorological factors, such as surface temperature, temperature, precipitation, and evaporation. Tang et al. [76] analyzed and verified the feasibility and practicability of MODIS–NDVI products in desert areas through meteorological factors.

3.3.3. Vegetation Estimation Model

Numerous scholars have developed remote sensing estimation models for vegetation coverage by fitting various NDVI data. The formulas and indicators of these models are presented in Table 3.

Based on the analysis of the correlation between the vegetation coverage and NDVI index using the MODIS–NDVI data method, it was observed that the linear model exhibited the highest accuracy ($R^2 = 0.930$). The linear model was selected to invert the vegetation coverage in the interior and marginal areas of the desert. Then, a spatial inversion model of the MODIS–NDVI data and the vegetation coverage of the quadrat was established.

It is helpful for us to grasp the characteristics of the vegetation in the desert, as well as the response of the vegetation to temperature and precipitation. Among them, it can be concluded that, in the fitting equation of the GF2 NDVI and vegetation coverage, the polynomial fitting effect was shown to be the best, followed by the linear fitting. Although the polynomial fitting increases with the degree, the coefficient of determination R^2 also continues to increase. However, since the coefficient of the high-order polynomial term is negative, as the x value (NDVI) increases, the y value (vegetation coverage) will have a downward inflection point near 30 or slightly greater than 20, which is obviously inconsistent with common sense. Therefore, choose the linear equation $y = 149.86x - 13.449$ ($R^2 = 0.7353$). In the fitting equation between the ZY1-02C NDVI and the vegetation coverage, the polynomial fitting effect was the best (As shown in the Table 3). The polynomial equation $y = 97.397x_2 + 80.837x - 5.2109$ ($R^2 = 0.818$) was selected as the remote sensing estimation model of the vegetation coverage based on the ZY1-02C NDVI. By combining UAV images with high-resolution data and corresponding statistical units, the method successfully addresses the uncertainty associated with previous point-based data measurements. Notably, there exists a significant correlation between precipitation, evaporation, and the FVC (fractional vegetation cover). However, the interaction between temperature, surface temperature, precipitation, and evaporation also exerts a considerable influence on the FVC.

Table 3. Regression models between vegetation coverage and the NDVI: (x —NDVI; y —vegetation coverage (%); T —temperature; P —precipitation; L —land-surface temperature; V —evaporation; “:” —interaction.).

Types of NDVI	Study Area	Type of Model	Model Equation	R^2	References
MODIS _{NDVI}	Badain Jaran Desert	Linear function	$y = 124.62x - 4.998$	0.930	[26]
		Quadratic polynomial	$y = 60.932x^2 + 82.141x - 0.307$	0.920	
		Logarithm function	$y = 27.226\ln x + 73.203$	0.780	
		Exponent function	$y = 4.370 \times 10^{5.024x}$	0.760	
		Power function	$y = 136.087x^{1.283}$	0.860	
GF2 _{NDVI}	Gurban tunggut Desert	Linear function	$y = 149.86x - 13.449$	0.735	[27]
		Quadratic polynomial	$y = -311.85x^2 + 251.03x - 21.138$	0.742	
		Logarithm function	$y = 22.929\ln x + 53.236$	0.734	
		Exponent function	$y = 0.203 \times 10^{22.291x}$	0.444	
		Power function	$y = 5120x^{3.5206}$	0.473	
ZY1-02C _{NDVI}	Karamay Desert	Linear function	$y = 118.9x - 8.4998$	0.816	[27]
		Quadratic polynomial	$y = 97.397x^2 + 80.837x - 5.2109$	0.818	
		Logarithm function	$y = 20.468\ln x + 49.22$	0.770	
		Exponent function	$y = 1.7665 \times 10^{9.7935x}$	0.778	
		Power function	$y = 236.74x^{1.7639}$	0.805	
FVC _R	Alxa	Stepwise regression	$FVC_R = -10.53 + 1.939T + 0.01585P - 0.001559T : V + 0.0002772V : L - 0.001559T : P - 0.06309T : L$	0.736	[76]
FVC _M	Alxa	Stepwise regression	$FVC_M = -0.9219 - 0.002354V + 0.5962T + 0.001268P + 0.0001761V : L - 0.038T : L$	0.834	[76]

3.3.4. Limitations

The establishment of NDVI remote sensing estimation models can provide valuable services and references for ecological monitoring and research in desert areas to a certain extent. Currently, despite the numerous NDVI data that have been fitted to develop the remote sensing estimation models of vegetation coverage, the stability of the NDVI data remains insufficient, thereby leading to lower accuracy in the model estimation and some errors. These limitations necessitate further improvements. Although satellite remote sensing technology has been extensively applied for vegetation coverage inversion,

there are certain drawbacks when evaluating the authenticity of the inversion results. To accurately assess the vegetation coverage, it is imperative to gain a deeper understanding of the relationship between the vegetation coverage and meteorological factors, as well as the composition, structure, and dynamics of the desert vegetation. Such knowledge is crucial for enhancing the evaluation of vegetation coverage accuracy and gaining insights into the complexities of desert vegetation.

3.4. Classification of Plant Community Types

A plant community type can be defined as a grouping of plant types that exhibit interconnected relationships between species and their environments. In the context of dryland systems, integrating sparse desert vegetation and bare surfaces into comprehensive cover complexes is essential for understanding the underlying biophysical processes, as well as for ensuring sustainable management and decision making [8,9]. This integration plays a critical role in sand fixation, carbon sequestration, and the overall ecosystem stability in deserts and oases [77,78]. Differentiating community types is highly valuable and has found applications in various desert-related fields. However, further breakthroughs in this area of research are currently needed to advance our understanding.

3.4.1. Classical Methods

The multi-angle method has been applied in the mapping of desert steppe vegetation types. The multiangle imaging spectroradiometer (MISR) provides four spectral bands and nine angular reflectances. Su et al. [79] searched for the best combination of MISR multiangle data through multiangle reflectivity, surface anisotropy patterns, and support vector machine algorithms. The research sought to extract more useful information from the MISR data. It promoted the differentiation of desert vegetation types.

In order to reduce the misclassification of dryland cover, Sun [28] combined the cross-wavelet transform (XWT), logistic regression, and EM to conduct experiments. They first established the XWT to quantify the interactive features in the EM time-series pairs. Then, the research integrated the feature parameters in the EM pairs through principal component analysis (PCA) to reduce the dimensionality and to solve the multicollinearity. It used logistic regression to map and characterize the desert vegetation–habitat complex. Finally, this process was compared with other advanced machine-learning methods. This method could effectively reproduce the desert vegetation–habitat complex. It also has the potential to accurately monitor highly heterogeneous dryland landscapes.

Shrubs abound in the Gobi desert. In its ecosystem, its productivity is assessed by monitoring the AGB. Based on UAV RGB images, Ding et al. [80] used the visible vegetation index to estimate AGB of the shrub communities in Gobi Desert. The real-time control of the AGB is beneficial to protect and improve the Gobi Desert ecosystem.

3.4.2. Limitations

The complex relationship between the desert vegetation and the habitat in dryland systems [8] directly impacts the stability of desert oasis ecosystems [77,78]. A key focus of this research is the detailed classification of sparse vegetation and bare land, as it determines the potential degradation of the dryland system [8,9].

When studying the aboveground biomass (AGB) of vegetation, relying solely on vegetation coverage as a single index is insufficient. It is beneficial to incorporate investigations into community types to enhance the estimation of vegetation the AGB across different types.

3.5. Summary and Prevention Measures

The study of desert mobility aims to differentiate mobile deserts from nonmobile deserts in order to implement sand fixation and control measures for mobile desert areas. The primary distinction between mobile deserts and nonmobile deserts lies in their vegetation cover. This chapter initially introduces the visual interpretation method to provide a

preliminary assessment of the desert vegetation coverage, thereby enabling the classification of mobile deserts for further investigation. However, visual interpretation is subjective, time-consuming, and labor-intensive, thus imposing certain limitations. To obtain a more accurate understanding of the vegetation conditions in mobile deserts, spectral mixture analysis was employed to monitor the photosynthetic and nonphotosynthetic vegetation coverage. However, some deviations exist in this study, thus requiring further evaluation and confirmation. Lastly, fitting the NDVI index to establish a remote sensing estimation model for vegetation coverage enables more precise monitoring of vegetation growth in the desert. These research methods highlight the importance of the stability and accuracy in the model, thus pointing towards future research directions.

Monitoring the vegetation coverage allows for the identification of the mobile desert's extent and facilitates the implementation of appropriate control measures. Examining the photosynthetic and nonphotosynthetic characteristics of vegetation aids in studying the degradation mechanism of desert vegetation, as well as in selecting suitable species for sand fixation and control. The application of remote sensing estimation models in desert regions enables the timely adjustment of control strategies based on the vegetation growth status and trends, thereby transforming mobile deserts into nonmobile ones and reducing their detrimental effects.

4. Desertification Monitoring

Desertification is a multifaceted process of land degradation [81]. It involves the gradual deterioration of the soil organic matter content and a progressive reduction in the vegetation and water coverage on the soil surface. As a result, land productivity experiences a decline or loss, thereby significantly impacting the sustainable development of both the economy and the ecological environment [82]. To address this issue, various technical approaches have been employed to systematically observe and monitor indicators that are relevant to land degradation, thereby providing insights into the phenomenon. These observations, conducted at regular intervals and irregular intervals, have focused on key indicators that are of concern to humanity and can effectively reflect the occurrence of land degradation.

4.1. Desert Area Change Monitoring

4.1.1. Classical Methods

Desertification is a significant ecological and environmental issue that has garnered widespread attention in the contemporary world. Traditional methods for monitoring desert dynamics suffer from limitations such as long monitoring periods and limited coverage. However, with the advancement and widespread use of remote sensing technology, monitoring temporal and spatial changes in deserts has become faster and more objective [83,84]. Remote sensing enables the efficient and objective assessment of desertification processes, thereby providing valuable insights into the dynamics of desert ecosystems on a larger scale and in a more timely manner.

In order to monitor the dynamic movement of sand dunes, a number of methods have been proposed to extract sand dunes from satellite images using remote sensing. The manual tracking of dune shapes on aerial photographs and satellite images is the most primitive method [85,86]. Manual tracking is a difficult task that takes time and effort. The automatic and semiautomatic extraction technology of dune detection comes into being. The interannual variation of large-scale desert areas can be obtained, which is of great significance for understanding the dynamic change laws and driving mechanisms of desertification. Chang et al. [29] evaluated the accuracy of the corrected desert area based on the interpretation results of remote sensing images of the Tengger Desert. Bandeira et al. [87] proposed a method to detect sand dune fields on the surface of Mars by automatically extracting local information from Mars orbiter camera images. This study used machine-learning methods to extract barchan dunes from the Martian surface using high-resolution satellite imagery [88].

For classification based on object extraction, many studies have used sliding windows to extract spectral features and texture features [89,90]. Pi et al. [10] proposed the DGC and 3D-CNN models to identify deserts and grasslands. Moghaddam et al. [11] used an MLP to classify the Isfahan desert using Landsat satellite images, and they obtained the land cover map of the Sejzy area. Ge et al. [91] used the ANN, RF, SVM, and KNN to analyze seven different land cover types in China's Dengkou Oasis. Based on Sentinel high-resolution remote sensing images, Du et al. [92] applied the CNN deep-learning algorithm to the remote sensing classification of aeolian sand landforms. The study monitored the area of different types of sandy landforms in the western part of the Horqin Sandy Land, such as longitudinal dunes, flat sandy land, mild undulating sand land, nest-shapes land, parabolic dunes, barchan dunes, and dune chains. From 2015 to 2020, the area of the sand dunes decreased by 89.27 km², and the effectiveness of sand protection was remarkable, which shows a transformation of this area from a desert to an oasis. Aydda et al. [93] presented an easy method based on the processing of Sentinel 2 data. The proposed processing techniques included band selection (band ratio, the redness index, and the crust index), band filtering using low-pass filter 3 × 3, data transformation using principal component analysis (PCA), unsupervised classification using k-means, expectation maximization (EM), and isodata algorithms, and image segmentation. Using an isodata algorithm to realize the automatic extraction of dunes resulted in high performance.

Remote sensing satellite images with different resolutions can meet certain classification requirements. The resolution of remote sensing satellite data is continuously advancing, thereby offering increasingly detailed and comprehensive information. Moreover, with the integration of emerging technologies, the capture and utilization of remote sensing information have been significantly enhanced [94]. These advancements in remote sensing technology have facilitated a more in-depth understanding and analysis of various environmental and ecological phenomena, including the monitoring and assessment of desertification. The improved resolution and richer information content of remote sensing data have opened up new possibilities for accurately detecting and characterizing subtle changes in desert ecosystems, thereby contributing to more effective management and conservation strategies.

4.1.2. Limitations

The research and control of desertification are essential for achieving sustainable development goals [95]. In this study, an object-oriented approach combined with human-computer interaction interpretation was employed to classify and map the dynamic changes in sandy land. This methodology allows for the analysis of spatial and temporal evolution characteristics. The specific processing workflow is illustrated in Figure 6. The preprocessed data bands were fused, followed by classification. A comparison was made between the resulting data and the spatial distribution images of the interannual area sequence to assess the area error. Through iterative refinement, a revised interannual sequence of the desert area was ultimately obtained, thereby providing valuable insights into the ongoing changes and trends in desertification.

Compared to previous studies [96,97], the collaborative approach of object-oriented classification [98] and human-computer interactive interpretation [99] have effectively addressed the challenge of identifying sparse vegetation areas with subtle spectral characteristics. By utilizing the spectral, spatial, and thematic features of remote sensing images, a comprehensive extraction of land use/cover information was achieved. However, it should be noted that the utilization of the MODIS data in this study involved two different resolutions: medium and low [100–102], which may have introduced errors in the extraction and monitoring of the sandy land and vegetation coverage. Thus, further research is required to continuously improve the accuracy.

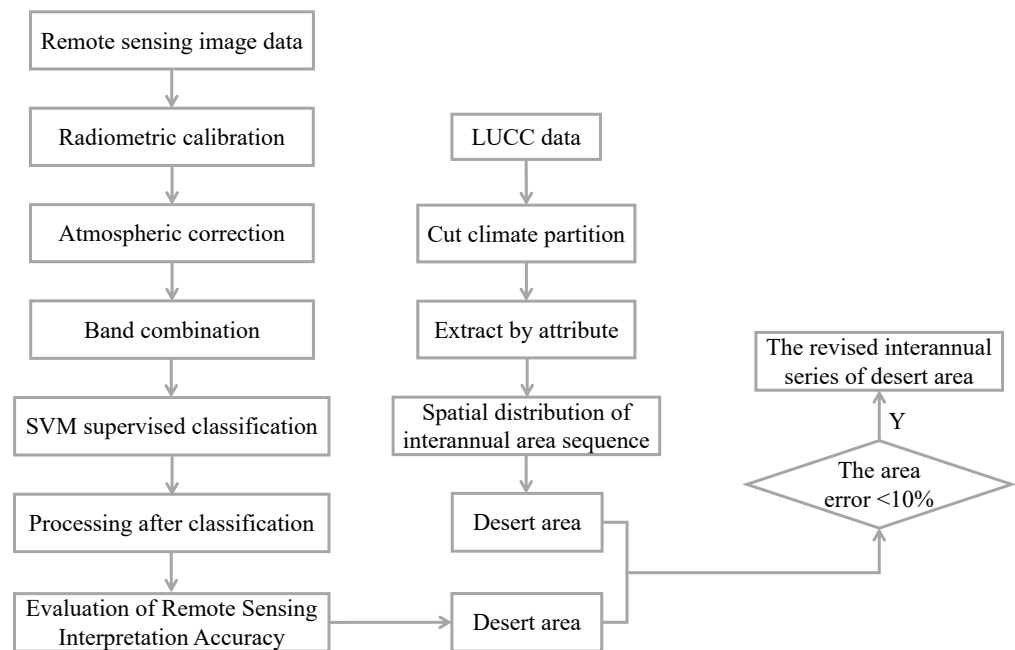


Figure 6. Accuracy evaluation of desert area based on remote sensing images.

In future investigations, the focus will be on optimizing the image data resolution and refining the computer algorithms. There remains ample room for exploration and application. The next step involves optimizing deep-learning parameters in convolutional neural networks and integrating long-term images, meteorological data (including wind direction, temperature, and precipitation), and human activity factors. These additions will enable remote sensing classification, dynamic evolution analysis, and the identification of the driving factors related to the long-term of sandy landform types. These methods aim to fully leverage the information contained within remote sensing images and enhance the accuracy of land classification, particularly in high-resolution images. However, challenges such as time-consuming calculations and inaccurate edge segmentation results need to be addressed. Future research should fully utilize image segmentation techniques to overcome these issues. Additionally, it is crucial to validate the proposed methodology using high-resolution images to detect smaller barchan dunes that might have been missed in the previous unsupervised classification studies. Moreover, exploring other bands, ratios, and indices that are suitable for the different mineralogical compositions of sand dunes would serve as a valuable supplementary study to improve the detection of various types of sand dunes.

4.2. Remote Sensing Ecological Index

The evaluation of the ecological environment in mobile deserts requires the use of an RSEI. As research in this field progresses, there has been a continuous increase and optimization of the indices that are applicable for this purpose. Additionally, new algorithms that are suitable for RSEI calculation continue to emerge, thereby contributing to the advancement of this research area.

4.2.1. Background

The RSEI is calculated by integrating four key indices—greenness, dryness, humidity, and heat—using a principal component analysis. The first principal component is then selected as the RSEI value. Jiang et al. [103] conducted a study using remote sensing images from 2006 and 2017 by employing the RSEI proposed by Xu [12]. To assess the ecological environment of the Gurbantunggut Desert, the researchers selected four ecological factors, namely, the NDVI, wet, the LST, and the NDSI, which are known to reflect the quality of

the ecological environment. These factors were utilized to construct a dynamic evaluation system for the remote sensing ecological index. The multivariate statistical method of principal component transformation was employed to combine the aforementioned indices, and the normalized PC1 was used to generate the RSEI.

The RSEI expression was defined as follows: $RSEI_0 = 1 - PC1[f(NDVI, Wet, LST, NDSI)]$. To facilitate the contrast between the different indicators, $RSEI_0$ can be normalized as $RSEI = (RSEI_0 - RSEI_{0min}) / (RSEI_{0max} - RSEI_{0min})$. Its value is between [0, 1]. According to the existing grading standards, the normalized RSEI was divided into 0–0.2, 0.2–0.4, 0.4–0.6, 0.6–0.8 and 0.8–1 at an interval of 0.2 corresponding to five ecological grades: Worst, Worse, Middle, Good, and Excellent, respectively. The value of the RSEI is positively correlated with ecological quality. This classification method of intervals can provide a rough understanding of the ecological environment conditions in this area to some extent. To obtain a more accurate assessment, further research is needed to determine the specific numerical values for each level of environmental condition classification.

Moreover, the study examined the spatial and temporal variations and patterns of the ecological environment quality in Gurbantunggut Desert. Although the overall ecological quality of the Gurbantunggut Desert displayed a declining trend, certain areas exhibited improved ecological quality, particularly in the densely vegetated northeastern region and the irrigation area along the southern border. These findings will serve as a foundation for future scientific and effective environmental protection and management initiatives.

4.2.2. Classical Methods of Indices

In order to better monitor and evaluate the ecological quality, researchers used a variety of indices for assessment. Table 4 lists the equations for each feature. After data preprocessing, the vegetation, soil, surface radiation, and texture information can be characterized by the feature index combining spectral features and texture features. The indices include the NDVI, the soil-adjusted vegetation index (SAVI), the enhanced vegetation index (EVI), the 2-band EVI (EVI2), the modified soil adjusted vegetation index (MSAVI), the soil moisture monitoring index (SMMI), the topsoil grain size index (TGSI), the visible atmospherically resistant index (VARI), the index-based built-up index (IBI), the bare soil index (BSI), the normalized different bare soil index (NDBSI), the albedo, the brightness, the greenness, the wetness, the mean, the variance, the homogeneity, the contrast, the dissimilarity, the entropy, the angular second moment and correlation, etc.

Table 4. Characteristic computational formulas (ρ_{Blue} , ρ_{Green} , ρ_{Red} , ρ_{NIR} , ρ_{SWIR1} , and ρ_{SWIR2} correspond to blue, green, red, near infrared, short infrared 1, and short infrared 2 bands of the remote sensing satellite images, respectively. L —soil adjustment factor; $p(i, j)$ ($i, j = 0, 1, 2, \dots, N - 1$)—grayscale co-occurrence matrix; N —image gray level; and i, j —pixel gray value.)

Characteristic Index	Computational Formula	References
NDVI	$NDVI = \frac{\rho_{NIR} - \rho_{Red}}{\rho_{NIR} + \rho_{Red}}$	[104]
SAVI	$SAVI = (1 + L) \frac{\rho_{NIR} - \rho_{Red}}{\rho_{NIR} + \rho_{Red} + L}$	[105]
EVI	$EVI_{MODIS} = 2.5 \frac{\rho_{NIR} - \rho_{Red}}{\rho_{NIR} + 6\rho_{Red} - 7.5\rho_{Blue} + 1}$	[105]
EVI2	$EVI2_{MODIS} = 2.5 \frac{\rho_{NIR} - \rho_{Red}}{\rho_{NIR} + 2.4\rho_{Red} + 1}$	[105]
MSAVI	$MSAVI = \frac{2\rho_{NIR} + 1 - \sqrt{(2\rho_{NIR} + 1)^2 - 8(\rho_{NIR} - \rho_{Red})}}{2}$	[106]
SMMI	$SMMI = \sqrt{\frac{\rho_{NIR}^2 + \rho_{Red}^2}{2}}$	[107]
TGSI	$TGSI = \frac{\rho_{Red} - \rho_{Blue}}{\rho_{Red} + \rho_{Blue} + \rho_{Green}}$	[108]
VARI	$VARI = \frac{\rho_{Green} - \rho_{Red}}{\rho_{Green} + \rho_{Red} - \rho_{Blue}}$	[109]
IBI	$IBI = \frac{2\rho_{SWIR1}}{\rho_{SWIR1} + \rho_{NIR}} - \left(\frac{\rho_{NIR}}{\rho_{NIR} + \rho_{Red}} + \frac{\rho_{Green}}{\rho_{Green} + \rho_{SWIR1}} \right)$	[110]
BSI	$BSI = \frac{2\rho_{SWIR1}}{\rho_{SWIR1} + \rho_{NIR}} + \left(\frac{\rho_{NIR}}{\rho_{NIR} + \rho_{Red}} + \frac{\rho_{Green}}{\rho_{Green} + \rho_{SWIR1}} \right)$	[111]
NDBSI	$NDBSI = \frac{(\rho_{SWIR1} + \rho_{Red}) - (\rho_{NIR} + \rho_{Blue})}{IBI + BSI}$	[112]

Table 4. Cont.

Characteristic Index	Computational Formula	References
Albedo	$Albedo = 0.356 \times \rho_{Blue} + 0.13 \times \rho_{Red} + 0.373 \times \rho_{NIR} + 0.085 \times \rho_{SWIR1} + 0.072 \times \rho_{SWIR2} - 0.0018$	[113]
Brightness	$Brightness_{Landsat5} = 0.33183 \times \rho_{Blue} + 0.33121 \times \rho_{Green} + 0.55177 \times \rho_{Red} + 0.42514 \times \rho_{NIR} + 0.48087 \times \rho_{SWIR1} + 0.25252 \times \rho_{SWIR2}$ $Brightness_{Landsat8} = 0.3029 \times \rho_{Blue} + 0.2786 \times \rho_{Green} + 0.4733 \times \rho_{Red} + 0.5599 \times \rho_{NIR} + 0.508 \times \rho_{SWIR1} + 0.1872 \times \rho_{SWIR2}$	[114]
Greenness	$Greenness_{Landsat5} = -0.24717 \times \rho_{Blue} - 0.16263 \times \rho_{Green} - 0.06239 \times \rho_{Red} + 0.85468 \times \rho_{NIR} + 0.05493 \times \rho_{SWIR1} - 0.11749 \times \rho_{SWIR2}$ $Greenness_{Landsat8} = -0.2941 \times \rho_{Blue} - 0.243 \times \rho_{Green} - 0.5424 \times \rho_{Red} + 0.7276 \times \rho_{NIR} + 0.0713 \times \rho_{SWIR1} - 0.1608 \times \rho_{SWIR2}$	[114]
Wetness	$Wetness_{Landsat5} = 0.13929 \times \rho_{Blue} + 0.22490 \times \rho_{Green} + 0.40359 \times \rho_{Red} + 0.25178 \times \rho_{NIR} - 0.70133 \times \rho_{SWIR1} - 0.45732 \times \rho_{SWIR2}$ $Wetness_{Landsat8} = 0.1511 \times \rho_{Blue} + 0.1973 \times \rho_{Green} + 0.3283 \times \rho_{Red} + 0.3407 \times \rho_{NIR} - 0.7117 \times \rho_{SWIR1} - 0.4559 \times \rho_{SWIR2}$	[114]
Mean	$Mean = \sum_i \sum_j i \times p(i, j)$	[114]
Variance	$Variance = \sum_i \sum_j (i - \mu)^2 p(i, j), \mu = Mean$	[114]
Homogeneity	$Homogeneity = \sum_i \sum_j \frac{p(i, j)}{1 + i - j }$	[114]
Contrast	$Contrast = \sum_n n^2 \{ \sum_i \sum_j p(i, j) \}, n = i - j $	[114]
Dissimilarity	$Dissimilarity = \sum_i \sum_j p(i, j) \times i - j $	[114]
Entropy	$Entropy = \sum_i \sum_j p(i, j) \log p(i, j)$	[114]
AngularSecondMoment	$AngularSecondMoment = \sum_i \sum_j p^2(i, j)$	[114]
Correlation	$Correlation = \frac{1}{\sigma_1 \sigma_2} \sum_i \sum_j (ij) p(i, j) - \mu_1 \mu_2, \mu = Mean, \sigma = Variance$	[114]

The multitemporal series of the EVI2 covering the period between 2000 and 2016 was used, which was calculated from data provided by the MODIS sensor carried aboard the Terra satellite. According to this, Bezerra et al. [115] proposed a methodology that contributed to the determination of the degree of the degradation through the determination of degradation trajectories. However, it must be complemented with additional information, such as trends and climatic scenarios of the land use and land cover with retrospective analysis of the landscape, soil erosion, field recognition, and socioeconomic information, among others. According to the actual situation of the Naiman Desert, Guo et al. [116] selected four sensitive indicators, including the MSAVI, NDVI, TGSi, and albedo, to construct five feature spaces. After that, experiments were conducted to compare the various desertification monitoring models in order to find a more accurate classification model. Among the feature space models used for the Naiman Desert, the albedo–MSAVI achieved the highest accuracy, which reached 90.1%. It was deemed most suitable for monitoring the desertification of the Naiman Desert.

The causes of desertification are complex, which include but are not limited to climate and human factors. Liu et al. [117] studied the desertification change in the eastern region from 2000 to 2015 by using the MODIS data for 15 years and combining multiple time nodes and desert stations. Liu et al. [118] used PCA to construct an improved remote sensing ecological index (MRSEI) that combined greenness, humidity, dryness, heat, and air quality indices. The research also used the entropy weight method to calculate the weight of each index in the pressure state response model. The ecological environment index was obtained through the weighted method and compared with the MRSEI and RSEI. At the same time, the integrated greenness, heat, humidity, and dryness indices were used to construct the nonlinear remote sensing ecological index (NRSEI) using kernel principal

component analysis (KPCA). Finally, the MRSEI and NRSEI were compared and analyzed with the commonly used RSEI.

Desertification has emerged as a prevalent ecological issue worldwide, particularly in Central Asia. Jiang et al. [119] conducted a spatial and temporal analysis of the desertification process from 1982 to 2012, wherein they employed an analytical hierarchy process and used four selected indices. Desertification is influenced by various drivers, which can vary depending on the vegetation type present. Consequently, it is essential to determine the specific types and weights of ecosystem driving factors based on the unique circumstances of each ecosystem. However, due to the limited availability of long-term serial data sets, the study focused only on four selected indices to monitor the desertification process, without considering other potential factors contributing to desertification. In future research, the inclusion of additional indicators represents a promising avenue for the further exploration and understanding of the desertification process. The use of the NDVI, wetness, NDBSI, and LSI by Zhang et al. [120] was performed to construct the RSEI. The seasonal and annual RSEI values were calculated for temporal analysis. This finding suggests that, when studying desert regions, the seasonal effects of the RSEI should also be taken into consideration, as the vegetation in different areas exhibits varying trends in the NDVI and wetness due to different growth periods.

4.2.3. Classical Methods of Algorithms

A variety of indices of research has gradually matured. At the same time, the algorithms used to integrate the various indices that are used to evaluate desertification degree are also maturing.

The spatial structure of a desert can predict the signs of desert change. In order to verify this, Hamada et al. [121] used the variogram function generated by the VARI to provide theoretical support for the correlation between them. Furthermore, LST maps can reflect desert characteristics to a certain extent [122–124]. The improvement of its resolution depends on downscaling through the random forest multiple remote sensing index (MIRF) [125]. The normalized difference dust index (NDDI) is suitable for desert identification in an oasis. Thus, the MIRF is efficient and accurate. Pan et al. [126] improved the MIRF algorithm and designed a remote sensing index that could characterize the desert characteristics in arid areas.

Many scholars have comprehensively compared and analyzed various desertification monitoring algorithms. Meng et al. [113] used six machine-learning methods, and the maximum entropy method had the best performance. By using the change in center of gravity and intensity analysis model, the study monitored the distribution and change in desertification in Mongolia from 1990 to 2020 and made a desertification map. Jiang [127] determined the potential occurrence range of desertification in China from 2000 to 2020 based on meteorological data, which calculated desertification monitoring indicators (albedo, LST, NDVI, and TGSi) using the MODIS data based on the Google Earth Engine platform, and they used four machine-learning models (minimum distance, SVM, classification and regression tree (CART), and random forest) for desertification monitoring. The results showed that the accuracy of both the random forest model and the CART with the combination of the four indicators was good, but the accuracy of the random forest was somewhat higher. Li et al. [114] applied eleven algorithms: multinomial logistic regression (MLR), linear discriminant analysis (LDA), quadratic discriminant analysis (QDA), CART, support vector machines (SVM), Naive Bayes classifier (NB), K-nearest neighbor (KNN), RF, extremely randomized trees (ERT), AdaBoost (AB), and gradient boosting machine (GBM). The change in desertification in the Ningdong region since 2000 was analyzed.

In current research, researchers strive to identify the optimal desertification monitoring approach by integrating multiple indicators and employing advanced algorithms. Feng et al. [128] conducted an 18-year study on desertification change in the Mu Us Desert and concluded that the combination of the random forest (RF) algorithm and four selected indices (albedo, NDVI, LST, and TGSi) to achieve the highest classification accuracy. This

finding highlights the effectiveness of the RF algorithm in conjunction with these specific indicators for monitoring desertification dynamics in the Mu Us Desert.

4.2.4. Limitations

Based on the current studies, it has been found that the modified remote sensing ecological index (MRSEI) effectively reflects the influence of the air quality spatial distribution on the ecological quality, while the nonlinear remote sensing ecological Index (NRSEI), considering the weak linearity or nonlinearity among indices, outperforms the linear-transformed RSEI. Integrating various indicators and algorithms in desertification research provides a crucial approach for achieving more accurate and efficient understanding, as well as the management of desertification. Considering the seasonal effects, future research on the changing trends of RSEI values in deserts holds significant value. In the future, the utilization of diverse artificial intelligence platforms can be explored to enhance desert monitoring and control.

Among the algorithms used, the maximum entropy method, random forest (RF), and support vector machine (SVM) demonstrate reliable and stable performance in desertification monitoring. RF, in particular, exhibits superior classification results and proves to be an effective method. To avoid reliance on land cover datasets, the NDSI–RF approach excludes this dataset, thereby providing greater convenience in the implementation and improving the resolution and accuracy of land surface temperature (LST) estimation. Despite the effective prevention and control measures implemented in severely desertified areas worldwide, regions that are prone to desertification and those experiencing mild desertification continue to expand annually. This remains a focal point for future research.

In summary, the integration of multiple indicators and algorithms in desertification research offers a promising avenue for the enhanced understanding and control of desertification. Future studies can explore the integration of artificial intelligence platforms for more advanced desert monitoring and management.

4.3. Extraction of Ground Object Information from Remote Sensing Images

With the continuous development of the society and economy, coupled with climate change and population growth, various complex factors such as excessive farming and overgrazing have contributed to the increasing prevalence of land desertification. Egypt, for instance, possesses very limited areas suitable for human habitation. Out of its vast expanse of one million square kilometers, only 50,000 square kilometers are inhabited [129]. Consequently, research on the prevention and control of land desertification through the extraction of ground object information remains a prominent and crucial topic within the scientific community [130].

4.3.1. Classical Methods

Desertification mainly occurs in the desert border areas [131]. Therefore, the extraction of desert areas can provide researchers with valuable reference information about desert areas so as to formulate strategies for sand prevention and control. It is very difficult to separate spectrally confused land cover classes in semiarid regions using medium-resolution remotely sensed data, as the spectral response of several classes (e.g., settlements, barren land, and fallow land) are highly similar. Ali et al. [132] contributed to the remote sensing literature by testing different Sentinel-2 bands, as well as the transferability of well-optimized CNNs, for semi arid land use and land cover (LULC) classification in semiarid regions. Dang et al. [133] used a variety of satellite remote sensing data, such as Landsat, SPOT and GF, and combined them with a variety of machine-learning methods to develop the regional dataset and soil erosion intensity database of the Kubuqi Desert from 1990 to 2020 in the study of land use in the desert. The combination of high-resolution data and ground sampling was very effective for mapping efficiency and information recognition.

Many scholars use different algorithms to extract the ground object information of different deserts. Liu et al. [30] proposed an improved multispectral desert superpixel

generation algorithm based on entropy weight, which improved the simple linear iterative cluster (SLIC) algorithm from the input spectral information and the selection of compactness factors. The research proposes a superpixel compactness factor adaptive algorithm. In complex regions with large spectral differences, the compactness factor becomes smaller, and the superpixel edge fit is enhanced. In areas with high uniformity and consistency, the compactness factor becomes larger, which maintains the compactness and regularity of the superpixel shape, thereby improving the edge fit of the superpixels in complex terrain areas. At the same time, a rough extraction algorithm of the desert area based on superpixel and random walk has been proposed to remove nondesert features that are far away from the desert. It also combines an algorithm for the removal of abandoned farmland and artificial buildings based on spatial structure rules. Finally, the nondesert features such as desert transition zone, the Gobi, and sand were removed by the NDDI. Most desert areas can be accurately extracted. Yu et al. [134] used an improved superpixel algorithm based on the compactness factor to quickly and accurately extract the boundary of the Kumtag Desert in Shanshan County. The research based on the extraction of medium-resolution multispectral remote sensing images at the desert boundary provided data support for the confirmation of natural resources.

Tian et al. [135] automatically obtained the deep-level features of multiband remote sensing images by establishing a convolutional neural network. Then the research carried out the green space extraction experiment in the Kubuqi Desert. Based on the characteristics of multiband remote sensing data, the research designed CNNs for feature extraction of raw data. It also fused the extracted features with the band features of the original image. The fused features were input to the SVM classifier for training and model selection. Then, the models were evaluated and compared. In order to classify deserts rapidly and accurately from remote sensing images, Wang et al. [136] proposed an MSRNet based on an attention mechanism. The network initially extracts features through a conventional convolutional network, and then goes through a multiscale residual module for further processing. At the same time, the network introduces an attention mechanism to establish dependencies, which enables the network to adaptively recalibrate.

4.3.2. Comparison of Different Algorithms

The detailed outcomes of different algorithms utilized to extract ground feature information from diverse desert regions are summarized in Table 5. The remote sensing data used in multiple distinct studies were all acquired from the Landsat 8 satellite.

From the findings presented in Table 5, it can be observed that the SVM, CNN, and MSRNet classification algorithms yielded relatively reliable results. Particularly, the MSRNet exhibited superior generalization capabilities and achieved a higher classification accuracy for multispectral desert remote sensing images. As presented in Table 6, while enhancing the overall classification accuracy, the MSRNet also demonstrated superior classification performance for some highly perplexing land types. Through training on samples I and II for desert land type classification, it was confirmed that the MSRNet achieved a high accuracy in rapid basic classification and detailed classification. Detailed classification results can be obtained from the model trained on sample II. Comparative analysis of the experimental findings revealed varying types and degrees of misclassification within different classification methods. The ResNext network yielded the least satisfactory results, thereby exhibiting confusion in classifying basic landforms. Xception demonstrated less accuracy in classifying water compared to other land types. In comparison to the previous two networks, GoogLeNet achieved better classification results for desert images, albeit it lacked the desired level of detail in processing to attain the expected accuracy.

Table 5. Desert area extraction algorithm performance index.

Desert Area	Algorithm	OA (%)	Kappa	References
Kubuqi Desert	SVM	-	0.975	[135]
	Decision tree C5.0	-	0.970	
	Naive Bayes	-	0.890	
	CNNs classifier	-	0.978	
Kubuqi Desert	Superpixel and random walk	91.500	0.830	[30]
	SVM	86.000	0.720	
	IRI	89.000	0.780	
Taklimakan Desert	Superpixel and random walk	93.500	0.870	[30]
	SVM	86.000	0.720	
	IRI	85.500	0.710	
Kumtag Desert	Superpixel and random walk	94.500	0.890	[30]
	SVM	91.500	0.830	
	IRI	74.500	0.700	
Kumtag Desert	Manual mapping	84.300	0.750	[134]
	SVM	90.800	0.830	
	Improved Superpixel Algorithm	93.500	0.880	
Xinjiang, China I	SVM	50.080	0.317	[136]
	Random Forest	83.980	0.785	
	VGG-BN	90.010	0.866	
	GoogLeNet	94.210	0.922	
	Inception-SE	95.040	0.934	
	MSRNet	95.980	0.946	
Xinjiang, China II	ResNext	89.380	0.875	[136]
	Xception	92.500	0.912	
	GoogLeNet	95.470	0.947	
	MSRNet	96.690	0.961	

Table 6. Classification accuracy on the sample test set. (Ds—Desert. Gl—Grassland; Wt—Water. Gb—Gobi. Mt—Mountain. Cl—Cloud. Sn—Snow. Bg—Background).

Sample	Network	Ds (%)	Gl (%)	Wt (%)	Gb (%)	Mt (%)	Cl (%)	Sn (%)	Bg (%)	References
I	SVM	74.86	53.87	-	19.05	-	-	-	43.36	[136]
	RF	89.21	80.81	-	83.52	-	-	-	80.66	
	VGG-BN	93.24	89.86	-	88.80	-	-	-	90.88	
	GoogLeNet	95.62	94.59	-	91.41	-	-	-	93.65	
	Inception-SE	95.82	95.72	-	92.97	-	-	-	94.75	
	MSRNet	96.81	95.95	-	94.53	-	-	-	96.69	
II	ResNext	91.06	91.59	85.51	87.04	91.18	85.82	93.20	-	[136]
	Xception	93.39	93.21	89.58	91.70	94.05	91.67	94.06	-	
	GoogLeNet	96.31	95.91	93.77	95.18	96.43	93.72	96.44	-	
	MSRNet	98.10	96.66	95.29	96.19	97.02	95.89	97.62	-	

4.3.3. Limitations

There are various methods available for the automatic classification of desert remote sensing images, among which the MSRNet yields the most effective results and demonstrates proficient feature generalization, extraction, and classification. This superiority stems from the fact that other methods often encounter issues such as boundary blurring and low correct detection rates. However, it is important to acknowledge that the MSRNet also has certain drawbacks, such as the increased complexity of computations, as well as a higher time and cost consumption due to the pursuit of more accurate outcomes.

In studies employing CNNs for semiarid LULC mapping, it is worth exploring other machine-learning and deep-learning methods that may achieve similar or even superior

performance under different circumstances. Factors to consider include the variations in training data size and the different types of LULC classes. This direction of research holds promise for the future. High-resolution remote sensing images exhibit complex distributions of ground objects, which often contain redundant information that is irrelevant to the current scene, which can hinder accurate scene classification. To address this challenge, Zhang et al. [137] proposed a scene classification method based on the sparse representation of the spike convolutional neural network (SCNN). By leveraging the sparse output characteristics of spiking neurons, the study designed an SCNN to eliminate irrelevant redundant information in remote sensing images and achieved sparse representation of the images. The research also introduced a back-propagation algorithm based on the pulse output cross-entropy loss function, thereby enabling the gradient descent to train the spiking convolutional neural network. This optimization process aims to realize the classification of remote sensing image scenes.

In the context of desertification prevention and control, the demands for accuracy and precision in desert classification are continuously increasing. Moreover, the uncertainty factors and external influences impacting desert areas introduce certain challenges to desert classification. The most advanced machine-learning methods for remote sensing information extraction often construct feature vectors through image band combinations and texture analysis. However, this approach has limitations in terms of its optional features and often requires excessive human intervention.

4.4. Summary and Prevention Measures

Desertification poses significant harm by depleting organic matter, vegetation, and water resources. Therefore, the regular monitoring of desertification is crucial. One of the most straightforward indicators is the measurement of the desert area. This chapter provides an overview of various supervised and unsupervised classification methods employed to monitor long-term changes in desert area sizes. However, image segmentation based on deep learning still faces challenges such as misclassification and time-consuming processes, thereby necessitating further optimization in this area in future studies. Remote sensing ecological indices utilize multiple environmental factors, including humidity and temperature, to evaluate the quality of the ecological environment. In this chapter, two main approaches are summarized: the utilization of different indices and the different algorithms utilized for desertification monitoring. The combination of diverse indices and algorithms has proven to yield better results for assessing and monitoring the quality of the desert ecological environment. Additionally, monitoring ground object information in desert regions is also of great importance. This chapter reviews various deep-learning-based classification methods for monitoring the distribution and changes in grassland, the Gobi, and mountain areas within the desert. Currently, the extraction of band and texture features is limited, and further exploration of additional desert-specific features is warranted.

During the desert control process, it is essential to establish a comprehensive and effective monitoring system to aid in the formulation of control plans and the timely evaluation of control outcomes. The effectiveness of prevention and control measures relies on the monitoring of regional area changes, environmental index data, and the ecological characteristics of ground objects. Based on such monitoring efforts, more precise and efficient control programs can be developed for subsequent implementation.

5. Types of Mobile Dunes

Desertification has emerged as a pressing ecological issue that garners considerable attention and concern from human society. Its detrimental effects pose a serious threat to human well-being and overall health. Desertification is widespread across the inland areas of northwest China, with sand dunes being the predominant landform in deserts and sandy regions. These sand dunes, which account for 96% of China's desert and sandy land area, result from the accumulation of sand debris under the influence of wind. Understanding and comprehending the key regional morphological characteristics of sand dunes, as well

as their formation and evolutionary patterns, are essential for various aspects such as the development of sand resources and the preservation of ecological environments. The adoption of efficient and rational methods for classifying and monitoring dune morphology becomes a necessary endeavor to safeguard oasis ecosystems. This effort holds significant value in the study of regional aeolian landform characteristics, the environmental processes governing their formation and evolution, and the judicious allocation of sand control measures.

5.1. Sand Dune Morphology Extraction and Recognition

5.1.1. Deep-Learning Morphology Recognition Model

The term “deep learning” introduces the field of machine learning and then introduces artificial neural networks [138]. The excellent classification effect of deep learning methods also makes this method popular. Convolutional neural networks are the most commonly used models in the field of image recognition and classification. In 2012, Krizhevsky et al. [139] used an improved deep convolutional neural network, AlexNet, in the ImageNet competition. In 2015, Long et al. [140] proposed fully convolutional neural networks (FCNs). These networks cancel the fully connected layers in the network and replace them with convolutional layers, which enables the neural network to realize image segmentation at the semantic level and deal with pixel-by-pixel classification. In 2016, He et al. [141] designed a residual network (ResNet) architecture with up to 152 layers, which is deeper than previous DNNs, while still reducing complexity and being easier to train. Convolutional neural networks, deep convolutional autoencoders, deep belief nets, etc. have also been applied in remote sensing image processing [142–144]. Hu et al. [145] designed a 5-layer convolutional neural network to classify images for spectral domain features. The effect was better than traditional SVM and other classification methods.

With the frequent use of high-resolution remote sensing images, their classification methods emerge endlessly. Liu et al. [146] used deep-learning models to complete the task of classifying ground objects in high-resolution images. Moreover, in their work was compared with SVM and ANN methods, and the comparison proved that deep learning can better mine ground object information in images. Yang et al. [147] combined deep learning with SVM, and used the advantages of both to significantly improve the performance of image feature classification. Gao et al. [148] integrated spatial semantic information into the deep learning model to achieve the accurate recognition of ground objects in high-resolution images. Zhao et al. [149] combined deep learning with object-oriented methods to extract deep features of ground object information using convolutional neural networks. At the same time, the research also uses the object-oriented method to extract the topology and shape information of the ground object information. The application of deep learning models improves the classification accuracy of the ground objects in high-resolution images, which has advantageous development prospects.

5.1.2. Sand Dune Form Monitoring

Sand dunes, which are characterized as hill-like or ridge-like formations, arise from the accumulation of sand particles under the influence of wind. They represent the predominant landform types in deserts and sandy areas, thus exhibiting a close connection with natural factors such as climate variations, wind patterns, and sand availability. As the investigation of aeolian landforms progresses, comprehensive research on sand dune morphologies has emerged, thereby encompassing the analysis of their distribution, classification, morphology, as well as their intricate relationships with the natural environment [13].

Scientists began to use remote sensing images to observe sand dunes and used various methods to analyze the relationship between dune types, sand sources, and wind conditions. Anthonson et al. [150] analyzed the sand dunes of the Danish coastline based on GIS and remote sensing technology. Then, the research explored the relationship between the morphological characteristics of sand dunes and their main influencing factors such as wind conditions and vegetation coverage, as well as their interrelationships with time changes.

Necsoiu et al. [151] used ASTER and SPOT images to model according to the Gaussian noise characteristics of the images, and they calculated the moving speed of the dunes. Brown et al. [152] used aerial photos to extract relative stereo mapping and established the DEM to analyze the morphological characteristics of the coastal dunes in Michigan, USA. Lyons et al. [153] conducted research in the Strzelecki Desert in Australia, wherein they focused on dune biology to find the relationship between dune morphology and ecology. Zhao et al. [14] first divided Chinese deserts (sandlands) into fixed, semifixed, and mobile dunes according to the mobility classification method, and they then subdivided them into crescent dunes and dune chains according to the morphological method. Li et al. [15] divided the north coast of the Luan River in China into horizontal dunes, crescent dunes, star dunes and flat sandy land.

Zhao [154] used the three deep convolutional neural network models of VGG16, VGG19, and ResNet50 to train a prepared dataset. Then, the research optimized the network model by training image slices at various scales to extract the high-level features of dune types. Their work realized the automatic classification of typical dune type information in the Gurbantunggut Desert and Taklimakan Desert based on deep-learning technology. The utilization of various deep-learning algorithms emerges as a crucial approach for extracting sand-dune-type information. Through the integration of deep learning and multi-scale segmentation, characteristic information of the five typical sand dunes can be effectively extracted, thus facilitating automatic classification. Furthermore, it extracted more detailed boundary information at the junction of the two dune types. This approach not only leverages the advantages of automatically extracting and learning deep features of dune types, but it also achieves precise extraction of the dune types.

Despite advancements, there remains ample room for research on sand-dune-type classification, and deep-learning-based algorithms for sand dune feature extraction and classification will encounter various challenges during their practical applications.

Barchan dunes represent the most prevalent type of dune. Elbelrhiti [155] analyzed the relationship between barchan dunes and wind direction changes through the long-term observations of barchan dunes in the Great Lakes region of the United States. Chang et al. [156] investigated the stability mechanisms of the top section of barchan dunes in the Hexi Desert, Gansu Province. In addressing diverse environmental disasters in the Yamalak Desert, Jia et al. [157] conducted a study on dune migration patterns, which focused on typical barchan dunes in the area. They constructed a digital elevation model of sand dunes based on extensive measured data and high-resolution remote sensing images.

By utilizing deep-learning models to identify and classify ground objects in images or high spatial resolution images, current research has achieved commendable recognition accuracy and effectiveness. It has demonstrated the feasibility of employing deep-learning models in conjunction with remote sensing images for ground object recognition. While numerous studies have been conducted on barchan dunes, the characterization and changes of these dunes in certain desert areas still lack sufficient investigation.

Regarding the stability of barchan dunes, it can be inferred that prevailing winds and opposing winds play a crucial role in determining their stability and influencing their shape. Conversely, the movement pattern of aeolian sand can also be observed through the behavior of dunes. Opposing winds cause the dunes to elevate in height, thereby leading to an increase in their volume and a subsequent decrease in their movement speed. These factors exhibit a power function relationship.

Despite the incomplete resolution of barchan dune stability, the present study establishes a foundation for further research and creates favorable conditions for the effective monitoring and control of deserts.

5.2. Sand Ridge Line Extraction and Recognition

5.2.1. Background

The morphological evolution of sand dunes serves as a valuable record of past near-surface wind conditions and environmental changes. However, the study of these charac-

teristics has been constrained by the challenges of low efficiency and high cost associated with large-scale sand ridge extraction.

In the early research, dunes are mainly divided into five shapes according to their shape and the number of falling sand slopes: crescent shape, linear shape, reverse shape, parabolic shape, and star shape [158,159]. This classification, which is mainly limited to dune morphology, cannot truly achieve the quantitative reconstruction of the relationship between the two. Hunter et al. [160] divided the sand dune shape into horizontal, oblique, and vertical according to the relationship between the sand ridge line trend and the synthetic wind direction of the sand-blowing wind, which solved the problem of quantifying the sand dune shape. Based on these understandings, Rubin et al. [161] improved the mathematical method of the relationship between the strike of the sand ridge line and the synthetic direction of the sand-moving wind. He proposed a mathematical model of Gross Bedform–normal Transport, and realized the quantitative study between the sand ridge line trend and the near-surface dominant wind direction.

Greater attention should be directed towards the research of sand ridge line extraction methods, which are continually undergoing optimization and updates. Presently, the extraction methods can be classified into three main types: differential operator edge detection, fuzzy operator edge detection, and wavelet transform edge detection. These methods play a crucial role in accurately identifying and delineating sand ridge lines in remote sensing images.

5.2.2. Differential Operator Edge Detection

Edge detection technology, as a research hotspot in digital image processing technology, has been well developed in the past decades, and some research results have been achieved. Research on edge detection algorithms began in the 1950s. In 1959, Julez [162] mentioned the concept of edge detection in his paper. In 1965, Roberts [163] researched edge detection technology and proposed the famous Roberts edge detection operator. In 1970, Prewitt [164] proposed the Prewitt operator. In 1973, Irwin Sobel proposed the Sobel edge detection operator. These three edge detection operators are all first-order differential operators. The detection accuracy will be reduced because the detected edges are wider [165].

In 1980, David Courtnay Marr and Ellen Hildreth proposed the Laplacian of the Gaussian operator. This method of calculating image edge points through second-order derivatives improves the deficiencies of the above three first-order differential operators. It is no longer necessary to refine the edge, but because of the addition of Gaussian filtering, the image cannot meet the requirements of positioning and filtering noise at the same time. In 1986, Canny [166] proposed the Canny edge detection operator, which is still widely used. In 2013, Xu et al. [167] optimized on the basis of the Canny operator. The algorithm first removes impulse noise using on–off median filtering, and then uses histogram concave analysis to determine a double threshold. In 2020, Han et al. [168] increased the number of direction templates of the traditional Sobel operator to eight by improvement. The adaptability of the algorithm is realized by combining the local and global thresholds.

Conventional differential operations often amplify image noise, which can adversely affect the performance of edge detection. To mitigate this issue, the Canny operator employs a smoothing filter prior to the differential operation, thus effectively reducing the impact of noise and enhancing the overall edge detection results.

5.2.3. Fuzzy Operator Edge Detection

In addition to differential operators, researchers have explored the use of fuzzy operator methods for edge detection. The fundamental concept involves mapping the image from the spatial domain to the fuzzy feature domain using a membership function. This is followed by a blur enhancement process that enhances the contrast of pixels on either side of the edge. The fuzzy domain is then transformed back into the data space through the inverse transformation of the membership matrix, ultimately extracting the image's edges.

In 1987, Lee et al. [169] defined a fuzzy minimal morphological edge detection operator. This operator is less sensitive to noise than dilation and erosion operations. In 2012, Mahesh et al. [170] proposed a morphological edge detection algorithm based on multi-structures and multiscales. This algorithm enhances the resistance to noise while preserving image details. In 2016, Ge [171] proposed an edge detection algorithm that combined the Canny operator and morphological operator, which obtained the final image edge by fusing the edges obtained by the two operators.

The edge detection method based on fuzzy theory offers advantages such as a narrow edge width and a high signal-to-noise ratio, thereby enabling the effective separation of objects from the background. However, it involves complex matrix operations and exhibits limited anti-noise performance.

5.2.4. Wavelet Transform Edge Detection

The high-frequency part of the image is subdivided on the time scale and the low-frequency part is subdivided on the frequency scale through a wavelet transform, which can meet the needs of effectively extracting local detail edge information under different resolutions. In 2011, Huang et al. [172] used wavelet decomposition to detect the edges of low-frequency subimages and high-frequency subimages using the improved morphological operator and wavelet modulus maxima algorithm, respectively, and they then fused the subedge images. In 2017, Zhang et al. [173] proposed an edge detection algorithm based on interpolation wavelet tower decomposition. They could detect more detailed edges by combining the interpolating conjugator with the Mallat tower decomposition algorithm. However, the existence of the fracture point of the dune ridge line was still inevitable. The research on the continuity and integrity of dune ridge line still needs to be further improved.

We proposed an edge detection method based on the Faber–Schauder wavelet lifting scheme for extracting dune ridge lines from an original image (Figure 7). The method involved decomposing the image and connecting the edge points using a predicted edge algorithm to obtain the final extraction result. Additionally, we performed sand ridge line extraction using the lifting wavelet and mathematical morphology techniques. For comparison, we evaluated classical edge detection operators such as Roberts, Sobel, Prewitt, LOG, and Canny operators, as well as other algorithms including multiscale edge detection based on wavelet transform, extreme value detection, mathematical morphology, ant colony algorithm, and phase consistency algorithm. The results obtained from the different edge detection algorithms using two dune region images are shown in Figures 8 and 9.

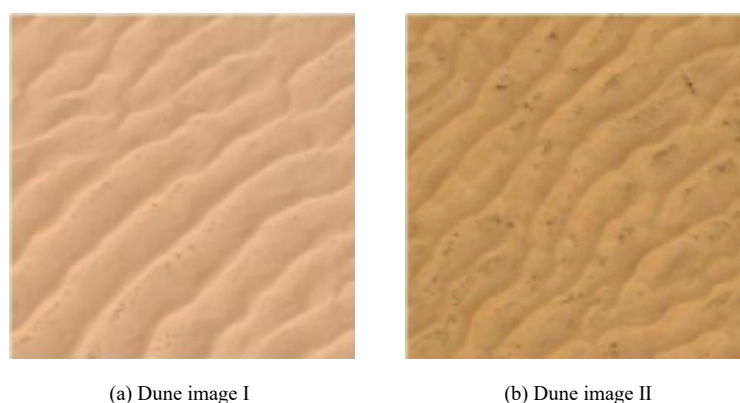


Figure 7. Dune image sample.

From the comparisons, it can be observed that the classical edge detection operators (Roberts, Sobel, Prewitt) extracted sand ridges with poor continuity and lost significant detail information. The LOG operator was sensitive to noise, and both the Canny and LOG operators produced pseudoedges rather than real sand ridges. The wavelet multiscale

edge detection algorithm achieved accurate sand ridge localization and noise suppression but exhibited slightly reduced continuity and integrity. The mathematical morphology algorithm preserved edge continuity but introduced false edge points. The extreme value detection algorithm struggled to detect high-curvature edges effectively. The ant colony algorithm resulted in numerous discontinuous ridges, and it had difficulty detecting weak edges while requiring significant computational time. The phase consistency algorithm was computationally intensive and susceptible to noise. The results obtained from these comparison algorithms exhibited unclear ridge locations, thus leading to significant errors in the analysis of the aeolian sand dynamics and geomorphic patterns.

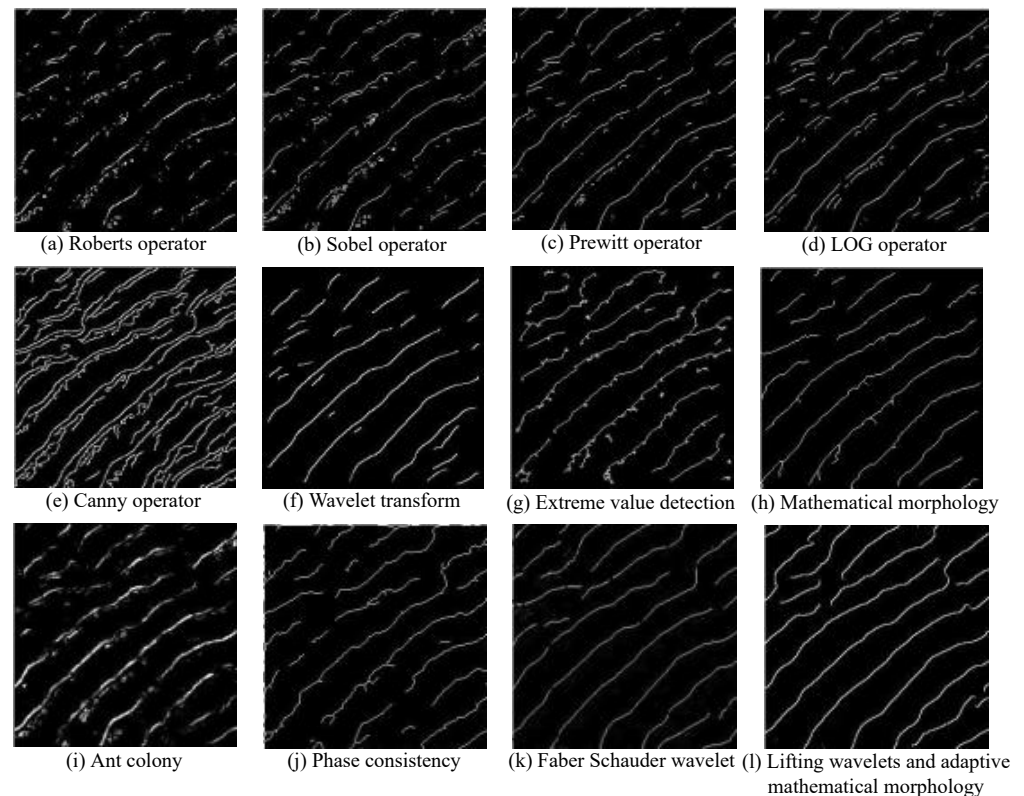


Figure 8. Dune ridge lines extraction results using different algorithms (Dune image I).

The Faber–Schauder wavelet algorithm demonstrated excellent performance in extracting dune ridge information. It preserved high continuity and integrity of the sand ridges, thereby making it suitable for calculating geomorphic pattern parameters and analyzing dynamic changes in deserts. Furthermore, the improved lifting wavelet and adaptive mathematical morphology algorithm yielded fewer breakpoints in the extracted dune ridges, thus ensuring continuity and integrity in the ridgeline extraction. This approach also exhibited better performance in extracting weak edges. This improvement was achieved by first using the improved mathematical morphology to extract edges from the low-frequency component of the image after lifting a wavelet transform, followed by edge extraction from the approximate part of the high-frequency component decomposed by the wavelet packet. These steps effectively suppressed the noise and enhanced the extraction of the dune ridge lines.

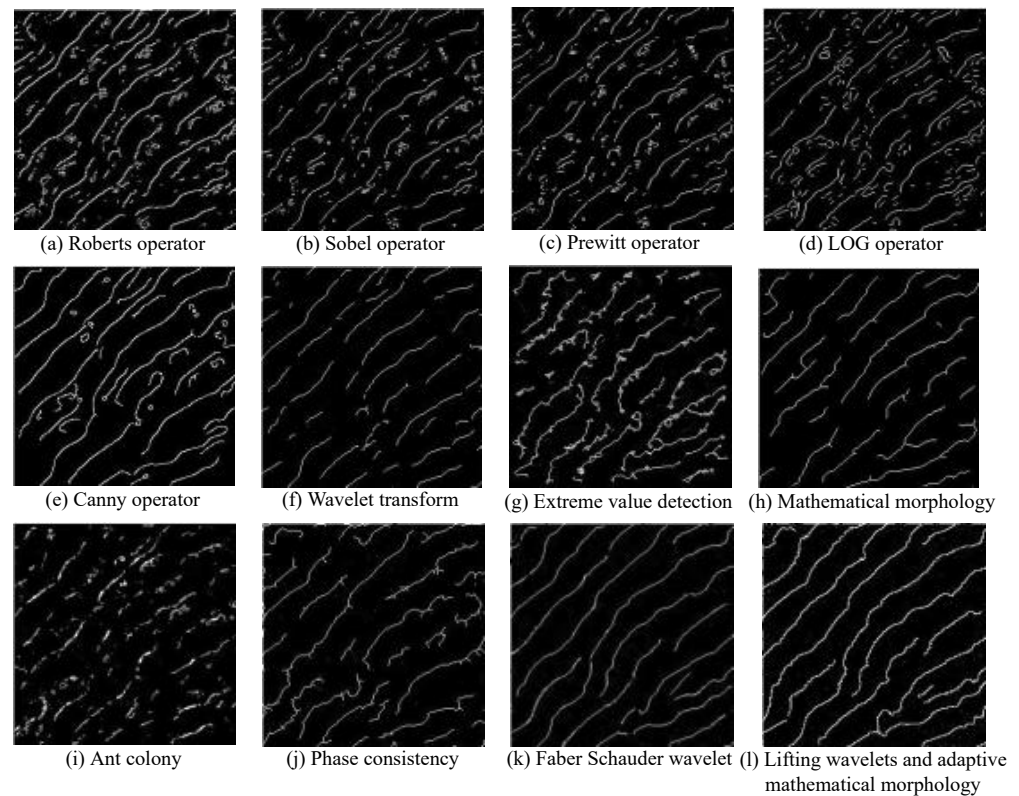


Figure 9. Dune ridge lines extraction results using different algorithms (Dune image II).

5.2.5. Other Methods

Modern edge detection techniques encompass various approaches, including neural-network-based edge detection, genetic-algorithm-based edge detection, multiscale edge detection, and subpixel edge detection. Jiang et al. [174] focused on the lateral dune area of the Tengger Desert as their research subject and extracted dune ridge lines from remote sensing images. Their approach relied on the grayscale difference between the dune windward slope and the falling sand slope in the remote sensing image to extract the sand ridge lines. Gao et al. [175] constructed a U-Net model based on a deep convolutional neural network, thereby enabling the efficient and accurate batch extraction of sand ridges. By incorporating data augmentation techniques, neuron random deactivation, batch normalization, and transfer learning, they achieved higher model accuracy during training and parameter updating.

While fuzzy edge detection and subpixel edge detection exhibit high accuracy, their performance regarding noise suppression is limited. On the other hand, methods based on neural networks and mathematical morphology edge detection address the issue of poor noise suppression but may not achieve sufficient detection accuracy. Further research is required to enhance the sand ridge line detection algorithm.

5.3. Summary and Prevention Measures

In the process of desert management, it is essential to utilize desert resources effectively. A comprehensive understanding of the geomorphic types, morphological characteristics, and evolution rules of deserts facilitates the development of sand resources and the protection of the ecological environment. This chapter provides a summary of the classification methods for dune morphology types and sand ridge extraction techniques. The current advancements in edge detection algorithms and classification/recognition using deep-learning models combined with remote sensing images have proven to be more effective. However, given the rapid progress of artificial intelligence, there is a constant emergence of lightweight and high-precision models, which present promising directions for future research.

Each dune type exhibits unique characteristics. The classification and monitoring of dune morphology discussed in this chapter contribute to desertification control strategies that are tailored to local conditions, resource allocation, and the preservation of the ecological environment.

6. Discussion

Extensive exploration and research have been conducted on deserts, and the application of remote sensing imagery combined with deep-learning methods has significantly advanced desertification monitoring and control. However, the current literature in this field lacks comprehensive integration and analysis. Considering the pressing need for the effective monitoring and control of desertification, this study initiates with remote sensing data and introduces various commonly used remote sensing datasets in desert research. Moreover, as desertification predominantly occurs in mobile desert regions, the study begins by analyzing and summarizing different research methods for distinguishing between mobile and nonmobile deserts. Once the mobile desert region is identified, a detailed study of its internal characteristics becomes possible. The study provides a comprehensive summary and analysis of the advanced and representative desert characteristics, ecological indicators, and detection methods for dune types, thus facilitating a thorough understanding of the research status and future development of desertification monitoring.

Furthermore, the study presents a range of high-quality and widely applicable desert remote sensing datasets that are available worldwide. These datasets serve as excellent resources for desertification monitoring and studies on desert mobility. Notably, the MODIS data has low spatial resolution, the GF satellite data offers high spatial resolution, and the Landsat satellite data, with its moderate resolution, is extensively employed in desert research. Although spatial resolution continues to improve, high resolution comes with the cost of larger data volumes. Hence, researchers can selectively choose appropriate data according to their specific research needs. The study also provides a detailed description of the preprocessing steps for each component of the desert remote sensing dataset. It is evident that preprocessing greatly reduces errors, thereby establishing optimal conditions for accurate desert studies. Additionally, many scholars combine desert remote sensing datasets with field survey data to construct sample datasets for comprehensive desert system research.

Deserts can be classified into mobile and nonmobile categories, where fixed deserts do not expand, while mobile deserts migrate and expand, thereby leading to desertification due to various factors. Currently, the most intuitive method for assessing desert mobility is visual interpretation, which aims to enhance vegetation protection and improve the ecological environment. However, this method has limitations in terms of misclassification, time consumption, and lacks intelligence and automation. In contrast, deep learning-based classification algorithms offer accurate and effective alternatives. Vegetation coverage serves as a crucial indicator for evaluating desert mobility. Many scholars have employed linear and nonlinear spectral hybrid models to estimate vegetation cover through spectral measurements, thus monitoring both photosynthetic and nonphotosynthetic desert vegetation. However, this method has limitations in effectively distinguishing between different vegetation types, and thus requires further improvement. Additionally, researchers have developed remote sensing estimation models for vegetation coverage by fitting various NDVI data. Moreover, differentiating community types serves as a classification approach involving known plant community types, thereby facilitating the monitoring of semiarid grasslands. The detailed monitoring of vegetation cover enables a more accurate assessment of the desertification extent and the formulation of effective prevention and control measures. The optimization of research models should not be overlooked. Nevertheless, the use of vegetation monitoring methods is constrained by the presence of vegetation, and the results are unreliable when studying areas with minimal vegetation in deserts.

To observe indicators reflecting desert conditions in the face of desertification, specific techniques need to be employed. Based on recent research on desertification monitoring,

it can be concluded that monitoring changes in desert areas and utilizing remote sensing ecological indices are fundamental and common approaches in desertification monitoring. Macrolevel monitoring of desert conditions holds great value, and future improvements can be made by combining different indices with diverse algorithms to enhance the effectiveness of the monitoring data acquisition. In order to achieve more precise control of desertification, desert classification serves as the foundation. Scholars have conducted feature information extraction research using deep learning techniques. Through the training of models and the utilization of convolutional neural networks combined with attention mechanisms, the classification of green spaces, lakes, and other features within deserts has been achieved. The generalization ability and classification accuracy of these models continue to improve, thus providing robust support for studying regional aeolian landform characteristics. However, the current feature information remains relatively limited, and further exploration of more comprehensive feature information is needed. Different desert regions exhibit distinct forms and types of deserts. In order to tailor desertification monitoring and control to local conditions, researchers have conducted detailed studies on different dune types. The deep-learning-based extraction of dune feature information is primarily employed for the classification of mobile dune morphology. However, studies on dune types are still imprecise. Sand ridge lines, which play a prominent role in dune classification, offer a favorable approach for such studies. Scholars have employed edge detection techniques to extract sand ridge lines, thereby continuously updating the model parameters of the detection and extraction algorithm to improve accuracy. Existing studies on barchan dunes have only discussed and analyzed a limited number of factors influencing their movement, including natural and desert-specific factors. Thus, the reliability of these studies requires further investigation. In future research, a comprehensive consideration of multiple factors and the introduction of lightweight and high-precision models are necessary for desert studies to effectively utilize desert resources and protect the ecological environment.

This study had several limitations. Firstly, the stability of NDVI data for desert mobility assessment is still lacking, thus resulting in reduced estimation accuracy of the model and necessitating further improvement. Additionally, there is a need for spatially refined methods to identify complex desert vegetation–habitat interactions, with considerable room for accuracy enhancement. Secondly, as a crucial research index, remote sensing ecological indices are indispensable in desertification monitoring. However, the selection of too many or too few parameters and monitoring algorithms can lead to poor monitoring outcomes. Future research should address the problem of determining the optimal combinations of parameters and algorithms. Lastly, the recognition and classification of dune types hold significant importance for studying dune stability, but the stability of dunes remains an unsolved scientific problem. In future research, remote sensing data with higher resolutions should be appropriately utilized in desert studies, thereby ensuring data quantity within acceptable limits to obtain more precise desert characteristic information and experimental accuracy. By selecting different indices from existing remote sensing ecological indices, the most suitable parameter combination and corresponding algorithm can be determined. The transformation from mobile deserts to nonmobile deserts remains an urgent issue to be resolved, and the development of lightweight and high-precision algorithms for dune feature extraction and classification based on deep learning will encounter numerous challenges.

7. Conclusions

The field of desertification monitoring and control, which utilizes remote sensing images combined with deep learning, has witnessed significant advancements. However, there is still ample room for improvement and optimization, thus necessitating a comprehensive summary and analysis. This review introduces various desert remote sensing datasets that are commonly used in desert research, as well as their preprocessing methods. Among these datasets, the Landsat satellite stands out as the most widely utilized due to

its high spatial resolution and moderate data volume. Looking ahead, the acquisition of remote sensing data with even better spatial resolution will be imperative to obtain more comprehensive desert characteristic information. The review also summarizes the recent methods for desert mobility assessment and techniques for monitoring desertification in mobile desert areas. These advancements have led to the more precise and rapid extraction of mobile desert regions, with a primary focus on vegetation monitoring within deserts. Particularly, there is a need to further optimize the stability and accuracy of vegetation coverage estimation models. However, existing research methods are no longer applicable for desert areas with minimal vegetation, thus necessitating the exploration of alternative approaches. Furthermore, in the pursuit of effective desertification control, the study reviews the current state of dune type recognition and classification. The application of deep-learning methods in recognizing and monitoring dune morphology and ridge lines enables the tracking of dune direction and velocity within a specific time frame, thereby providing critical and comprehensive information on the real-time state of the desert's ecological environment and ground objects. The effective and reliable monitoring of desert conditions plays a crucial role in desertification control, thereby highlighting the urgency to further enhance model efficiency and accuracy. Drawing from relevant work, this review points out the limitations of current research and offers suggestions for future endeavors. The aim is to ensure the implementation of ecosystem protection and sustainable development practices in desert regions based on scientific foundations.

Author Contributions: Conceptualization, Z.W.; resources, Y.Z.; writing—original draft preparation, Y.S.; writing—review and editing, Y.S.; supervision, Z.W.; project administration, Y.Z.; funding acquisition, Z.W. All authors have read and agreed to the published version of the manuscript.

Funding: This research was supported by the National Key R&D Program of China (No.2022YFF0711700).

Data Availability Statement: Data sharing is not applicable.

Conflicts of Interest: The authors declare no conflict of interest.

References

1. Lyu, Y.L.; Shi, P.J.; Han, G.Y.; Liu, L.Y.; Guo, L.L. Desertification Control Practices in China. *Sustainability* **2020**, *12*, 3258. [[CrossRef](#)]
2. Li, C.J. Desertification threatens human survival and development—Countries need to work together to combat the spread of deserts. *Globalization* **2014**, *34*, 52–60+78+133–134.
3. Chang, X. Remote Sensing Monitoring of Recent Desert Area Changes in China and Analysis of Climatic Factors. Master's Thesis, Nanjing University, Nanjing, China, 2019.
4. Li, D.J.; Xu, D.Y.; Wang, Z.Y.; Ding, X.; Song, A.L. Ecological compensation for desertification control: A review. *J. Geogr. Sci.* **2018**, *28*, 367–384. [[CrossRef](#)]
5. Li, J.; Shen, H.F.; Li, H.F.; Jiang, M.H.; Yuan, Q.Q. Radiometric quality improvement of hyperspectral remote sensing images: A technical tutorial on variational framework. *J. Appl. Remote Sens.* **2021**, *15*, 031502. [[CrossRef](#)]
6. Fan, D.; Ni, L.; Jiang, X.G.; Fang, S.F.; Wu, H.; Zhang, X.P. Spatiotemporal Analysis of Vegetation Changes Along the Belt and Road Initiative Region From 1982 to 2015. *IEEE Access* **2020**, *8*, 122579–122588. [[CrossRef](#)]
7. Zhang, X.Y.; Liu, Y.; Xu, B.R.; Jiang, Z.Y. Discussion on the Interpretation Method of Haloxylon ammonium Forest in Ulan Buhe Desert High-resolution Remote Sensing Image. *Remote Sens. Technol. Appl.* **2010**, *25*, 828–835.
8. Sun, Q.Q.; Zhang, P.; Sun, D.F.; Liu, A.X.; Dai, J.W. Desert vegetation-habitat complexes mapping using Gaofen-1 WFV (wide field of view) time series images in Minqin County, China. *Int. J. Appl. Earth Obs. Geoinf.* **2018**, *73*, 522–534. [[CrossRef](#)]
9. Sun, D.F.; Liu, N. Coupling spectral unmixing and multiseasonal remote sensing for temperate dryland land-use/land-cover mapping in Minqin County, China. *Int. J. Remote Sens.* **2015**, *36*, 3636–3658. [[CrossRef](#)]
10. Pi, W.; Du, J.; Liu, H.; Zhu, X. Desertification Grassland Classification and Three-Dimensional Convolution Neural Network Model for Identifying Desert Grassland Landforms with Unmanned Aerial Vehicle Hyperspectral Remote Sensing Images. *J. Appl. Spectrosc.* **2020**, *87*, 309–318. [[CrossRef](#)]
11. Moghaddam, M.H.R.; Sedighi, A.; Fasihi, S.; Firozjahi, M.K. Effect of environmental policies in combating aeolian desertification over Sejzy Plain of Iran. *Aeolian Res.* **2018**, *35*, 19–28. [[CrossRef](#)]
12. Xu, H.Q. A remote sensing index for assessment of regional ecological changes. *China Environ. Sci.* **2013**, *33*, 889–897.
13. Chen, Z.P.; Chen, Y.Z.; Liu, X.P. *Supersource of Desert Landform and Its Research Method*; Science Press: Beijing, China, 1962.
14. Zhao, S.Q. Overview of deserts and Gobi in China. *Geogr. Knowl.* **1960**, *11*, 145–151.
15. Li, C.X.; Chen, G.; Wang, X.Q. Study on Coastal Sand Sedimentation at the North Bank of Luanhu River. *J. Desert Res.* **1987**, *7*, 12–21.

16. Kuang, W.; Ma, Y.G.; Li, H.; Liu, C. Analysis on the intensity and trend of land degradation in Central Asia from 1999 to 2012. *Remote Sens. Land Resour.* **2014**, *26*, 163–169.
17. Theil, H. *A Rank-Invariant Method of Linear and Polynomial Regression Analysis*; Springer: Dordrecht, The Netherlands, 1950; Volume 53, pp. 386–392. 521–525. 1397–1412.
18. Sen, P.K. Estimates of the regression coefficient based on Kendall's tau. *J. Am. Stat. Assoc.* **1968**, *63*, 1379–1389. [[CrossRef](#)]
19. Ma, L.Y.; Cui, X.; Feng, Q.S. Dynamic change analysis of grassland vegetation coverage in southern Gansu from 2001 to 2011. *J. Grass Ind.* **2014**, *23*, 1–9.
20. Wang, P.; Luo, X.W.; Zhou, Z.Y. Review of Key Technologies for Remote Sensing Information Acquisition Based on Micro-UAV. *Chin. J. Agric. Eng.* **2014**, *30*, 1–12.
21. Sun, Z.Y.; Chen, Y.Q.; Yang, L. Low-altitude remote sensing of light and small unmanned aerial vehicles and its application progress in ecology. *J. Appl. Ecol.* **2017**, *28*, 528–536.
22. Berni, J.A.J.; Zarco-Tejada, P.J.; Suarez, L. Thermal and narrow band multispectral remote sensing for vegetation monitoring from an unmanned aerial vehicle. *IEEE Trans. Geosci. Remote Sens.* **2009**, *47*, 722–738. [[CrossRef](#)]
23. Bian, J.; Li, A.; Zhang, Z. Grassland fractional vegetation cover monitoring using the composited HJ-1A/B time series images and unmanned aerial vehicles: A case study in Zoige wetland, China. In Proceedings of the IEEE International Geoscience and Remote Sensing Symposium, Beijing, China, 10–15 July 2016; pp. 7193–7195.
24. Lu, B.; He, Y. Species classification using Unmanned Aerial Vehicle (UAV) -acquired high spatial resolution imagery in a heterogeneous grassland. *ISPRS J. Photogramm. Remote Sens.* **2017**, *128*, 73–85. [[CrossRef](#)]
25. Ge, J.; Meng, B.P.; Yang, S.X. Research on dynamic change monitoring of alpine grassland coverage based on UAV technology and MODIS remote sensing data—Taking the eastern region of the Yellow River as an example. *J. Grass Ind.* **2017**, *26*, 1–12.
26. Liu, C.; Zhao, W.; Liu, B.; Meng, Y.Y. Research on the distribution characteristics and dynamic changes of vegetation in the Badain Jaran Desert based on UAV and MODIS data. *J. Desert Res.* **2019**, *39*, 92–102.
27. Yue, J.; Mu, G.J.; Tang, Z.H.; Yang, X.F. Research on the empirical model of remote sensing estimation of vegetation coverage in Xinjiang desert area based on NDVI. *Arid Land Geogr.* **2020**, *43*, 153–160.
28. Sun, Q.Q.; Zhang, P.; Wei, H.; Liud, A.X.; You, S.C. Improved mapping and understanding of desert vegetation-habitat complexes from intraannual series of spectral endmember space using cross wavelet transform and logistic regression. *Remote Sens. Environ.* **2020**, *236*, 111516. [[CrossRef](#)]
29. Chang, X.; Lu, H.Y.; Lv, N.N.; Cui, M.C.; Li, H.N. Remote sensing monitoring and climate impact analysis of desert area change in China from 1992 to 2015. *J. Desert Res.* **2020**, *40*, 57–63.
30. Liu, X.G. Extraction Algorithm of Desert Area Based on Landsat 8 Image. Master's Thesis, Dalian Maritime University, Dalian, China, 2020.
31. Melichar, M.; Didan, K.; Barreto-Munoz, A.; Duberstein, J.N. Random Forest Classification of Multitemporal Landsat 8 Spectral Data and Phenology Metrics for Land Cover Mapping in the Sonoran and Mojave Deserts. *Remote Sens.* **2023**, *15*, 1266. [[CrossRef](#)]
32. Phiri, D.; Simwanda, M.; Salekin, S.; Nyirenda, V.R.; Murayama, Y.; Ranagalage, M. Sentinel-2 Data for Land Cover/Use Mapping: A Review. *Remote Sens.* **2020**, *12*, 2291. [[CrossRef](#)]
33. Chen, X.; Wang, T.; Liu, S.L.; Peng, F.; Tsunekawa, A.; Kang, W.P.; Guo, Z.C.; Feng, K. A New Application of Random Forest Algorithm to Estimate Coverage of Moss-Dominated Biological Soil Crusts in Semi-Arid Mu Us Sandy Land, China. *Remote Sens.* **2019**, *11*, 1286. [[CrossRef](#)]
34. Ali, E.; Xu, W.B.; Ding, X.L. Improved optical image matching time series inversion approach for monitoring dune migration in North Sinai Sand Sea: Algorithm procedure, application, and validation. *ISPRS J. Photogramm. Remote Sens.* **2020**, *164*, 106–124. [[CrossRef](#)]
35. Al-Ali, Z.M.; Abdullah, M.M.; Assi, A.A.; Alhumimidi, M.S.; Wasan, A.Q.S.; Ali, T.S. The immediate impact of the associated COVID-19's lockdown campaign on the native vegetation recovery of Wadi Al Batin Tri-state desert. *Remote Sens. Appl. Soc. Environ.* **2021**, *23*, 100557. [[CrossRef](#)] [[PubMed](#)]
36. Els, A.; Merlo, S.; Knight, J. Comparison of two satellite imaging platforms for evaluating sand dune migration in the Ubari sand sea (Libyan Fazzan). In Proceedings of the 36th International Symposium on Remote Sensing of the Environment (ISRSE), Berlin, Germany, 11–15 May 2015; Volume 47, pp. 1375–1380.
37. Guo, N.; Qing, J.Z. Analysis and information Extraction of sandstorm spectra from NOAA satellites. *Plateau Meteorol.* **2004**, *05*, 643–647+735–736.
38. Han, J.; Tao, Z.; Xie, Y.; Li, H.N.; Liu, Q.Y.; Guan, X.G. A Novel Radiometric Cross-Calibration of GF-6/WFV With MODIS at the Dunhuang Radiometric Calibration Site. *IEEE J. Sel. Top. Appl. Earth Obs. Remote Sens.* **2021**, *14*, 1645–1653. [[CrossRef](#)]
39. Tang, H.Z.; Xie, J.F.; Tang, X.M.; Chen, W.; Li, Q. On-Orbit Absolute Radiometric Calibration and Validation of ZY3-02 Satellite Multispectral Sensor. *Sensors* **2022**, *22*, 2066. [[CrossRef](#)] [[PubMed](#)]
40. Tang, H.; Xie, J.; Chen, W.; Zhang, H.; Wang, H. Absolute Radiometric Calibration of ZY3-02 Satellite Multispectral Imager Based on Irradiance-Based Method. *Remote Sens.* **2023**, *15*, 448. [[CrossRef](#)]
41. Zheng, W. Study on Modification of TURNER Atmospheric Correction Model and Its Application. Master's Thesis, Nanjing Normal University, Nanjing, China, 2005.
42. Sun, S.C. Comparison of Atmospheric Correction Models of Lunar Ground-based Observation Data. Master's Thesis, Jilin University, Jilin, China, 2018.

43. Zhang, Q.Y. Comparison of atmospheric correction for FLAASH and empirical linearity and reason analysis. In Proceedings of the 2017 Academic Conference of Geological Society of China, Hangzhou, China, 10–12 October 2017.
44. Pflug, B.; Richter, R.; de los Reyes, R.; Reinartz, P. Comparing Atmospheric Correction Performance For Sentinel-2 And Landsat-8 Data. In Proceedings of the IEEE International Symposium on Geoscience and Remote Sensing IGARSS, Yokohama, Japan, 28 July–2 August 2019; pp. 6433–6436.
45. de los Reyes, R.; Langheinrich, M.; Schwind, P.; Richter, R.; Pflug, B.; Bachmann, M.; Müller, R.; Carmona, E.; Zekoll, V.; Reinartz, P. PACO: Python-Based Atmospheric Correction. *Sensors* **2020**, *20*, 1428. [[CrossRef](#)]
46. Kalinskaya, D.V.; Papkova, A.S. Why Is It Important to Consider Dust Aerosol in the Sevastopol and Black Sea Region during Remote Sensing Tasks? A Case Study. *Remote Sens.* **2022**, *14*, 1890. [[CrossRef](#)]
47. Thomas, B.; Charlie, S.B.; Pieter, V. Measuring Sand Dune Migration Rates with COSI-Corr and Landsat: Opportunities and Challenges. *Remote Sens.* **2019**, *11*, 2423.
48. Hua, L.; Sui, H.G.; Ding, W.; Fu, H.B. Automatic Geometric Correction of Complex Sea Condition Remote Sensing Image Based on Decision Tree Classification. *IOP Conf. Ser.-Earth Environ. Sci.* **2019**, *326*, 012006. [[CrossRef](#)]
49. Wang, S.M.; Dou, A.X.; Ding, L.; Yuan, X.X. Low resolution remote sensing image processing and productions development for earthquake disaster monitoring application. *IOP Conf. Ser.-Earth Environ. Sci.* **2020**, *569*, 012007. [[CrossRef](#)]
50. Li, Q.Y.; Zhong, R.F.; Yang, C.K.; Zhao, K.; Zhang, C.C.; Li, Y. Geometric Quality Improvement Method of Optical Remote Sensing Satellite Images Based on Rational Function Model. *Remote Sens.* **2022**, *14*, 4443. [[CrossRef](#)]
51. Xie, L.; Meng, X.; Zhao, X.; Fu, L.; Sharma, R.P.; Sun, H. Estimating Fractional Vegetation Cover Changes in Desert Regions Using RGB Data. *Remote Sens.* **2022**, *14*, 3833. [[CrossRef](#)]
52. Miao, Y.; Zhang, R.; Guo, J.; Yi, S.; Meng, B.; Liu, J. Vegetation Coverage in the Desert Area of the Junggar Basin of Xinjiang, China, Based on Unmanned Aerial Vehicle Technology and Multisource Data. *Remote Sens.* **2022**, *14*, 5146. [[CrossRef](#)]
53. Chen, F.; Zhang, J.; Han, E.R. Soil microbial diversity in natural Haloxylon ammodendron forest in Urad and its relationship with soil properties. *J. Desert Res.* **2022**, *42*, 207–214.
54. Yi, W. The Haloxylon Forest Have been Long Gone. *Disaster Reduct. China* **2009**, *1*, 22–33.
55. Bastin, G.; Scarth, P.; Schmidt, M.; Abbott, B.; Chewings, V.; Sparrow, A. Separating grazing and rainfall effects at regional scale using remote sensing imagery: A dynamic reference-cover method. *Remote Sens. Environ.* **2012**, *121*, 443–457. [[CrossRef](#)]
56. Li, X.S.; Zhang, G.X.; Wang, J.Y.; Ji, C.C.; Sun, B.; Gao, Z.H. Comparison of Methods for Estimating Fractional Cover of Photosynthetic and Non-Photosynthetic Vegetation in the Otindag Sandy Land Using GF-1 Wide-Field View Data. *Remote Sens.* **2016**, *8*, 800. [[CrossRef](#)]
57. Guerschman, J.P.; Scarth, P.; Mcvicar, T.; Renzullo, L.J.; Malthus, T.J.; Stewart, J.B. Assessing the effects of site heterogeneity and soil properties when unmixing photosynthetic vegetation, non-photosynthetic vegetation and bare soil fractions from Landsat and MODIS data. *Remote Sens. Environ.* **2015**, *161*, 12–26. [[CrossRef](#)]
58. Okin, G.S.; Clarke, K.D.; Lewis, M.M. Comparison of methods for estimation of absolute vegetation and soil fractional cover using MODIS normalized BRDF-adjusted reflectance data. *Remote Sens. Environ.* **2013**, *130*, 266–279. [[CrossRef](#)]
59. Boardman, J.W. Automated spectral unmixing of AVIRIS data using convex geometry concepts. In Proceedings of the Summaries Annu JPL Airborne Geoscience Workshop, Washington, DC, USA, 25–29 October 1993.
60. Ji, C.C.; Jia, Y.H.; Gao, Z.H.; Wei, H.D.; Li, X.S. Nonlinear spectral mixture effects for photosynthetic/non-photosynthetic vegetation cover estimates of typical desert vegetation in western China. *PLoS ONE* **2017**, *12*, e0189292. [[CrossRef](#)] [[PubMed](#)]
61. Chen, X.; Vierling, L. Spectral mixture analyses of hyperspectral data acquired using a tethered balloon. *Remote Sens. Environ.* **2006**, *103*, 338–350. [[CrossRef](#)]
62. Vikhamar, D.; Solberg, R. Snow-cover mapping in forests by constrained linear spectral unmixing of MODIS data. *Remote Sens. Environ.* **2003**, *88*, 309–323. [[CrossRef](#)]
63. Theseira, M.A.; Thomas, G.; Sannier, C.A.D. An evaluation of spectral mixture modelling applied to a semiarid environment. *Int. J. Remote Sens.* **2002**, *23*, 687–700. [[CrossRef](#)]
64. Wu, C.; Murray, A.T. Estimating impervious surface distribution by spectral mixture analysis. *Remote Sens. Environ.* **2003**, *84*, 493–505. [[CrossRef](#)]
65. Bioucas-Dias, J.M.; Plaza, A.; Dobigeon, N.; Parente, M.; Du, Q.; Gader, P. Hyperspectral Unmixing Overview: Geometrical, Statistical, and Sparse Regression-Based Approaches. *IEEE J. Sel. Top. Appl. Earth Obs. Remote Sens.* **2012**, *5*, 354–379. [[CrossRef](#)]
66. Chen, Y.L.; Huang, X.T.; Huang, J.F.; Liu, S.S.; Lu, D.S.; Zhao, S. Fractional monitoring of desert vegetation degradation, recovery, and greening using optimized multi-endmembers spectral mixture analysis in a dryland basin of Northwest China. *GIScience Remote Sens.* **2021**, *58*, 300–321. [[CrossRef](#)]
67. Adams, J.B.; Smith, M.O.; Gillespie, A.R. Imaging spectroscopy: Interpretation based on spectral mixture analysis. In *Remote Geochemical Analysis: Elemental and Mineralogical Composition*; Pieters, C.M., Englert, P., Eds.; Cambridge University Press: New York, NY, USA, 1993.
68. Drake, J.J.; Settle, N.A. Linear Mixing and the Estimation of Ground Cover Proportions. *Int. J. Remote Sens.* **1993**, *14*, 1159–1177.
69. Niu, B.R.; Liu, J.R.; Wang, Z.W. Research on remote sensing information extraction of vegetation coverage in arid and semi-arid regions. *J. Wuhan Univ. (Inf. Sci. Ed.)* **2005**, *30*, 27–30.
70. Zhao, J.; Wang, X.M.; Li, D.C. Quantitative analysis of vegetation cover changes in Minqin oasis based on MODIS. *Arid Area Resour. Environ.* **2012**, *26*, 91–96.

71. Cheng, H.F.; Zhang, W.B.; Chen, F. Advances in researches on application of remote sensing method to estimating vegetation coverage. *Remote Sens. Land Resour.* **2008**, *20*, 13–18.
72. Asrar, G.; Myneni, R.B.; Choudhury, B.J. Spatial heterogeneity in vegetation canopies and remote sensing of absorbed photosynthetically active radiation: A modelling study. *Remote Sens. Environ.* **1992**, *41*, 85–103. [[CrossRef](#)]
73. Choudhury, B.J. Relationships between vegetation indices, radiation absorption and net photosynthesis evaluated by a sensitivity analysis. *Remote Sens. Environ.* **1987**, *22*, 209–233. [[CrossRef](#)]
74. Wang, X.H.; Li, Z.Y.; Gao, Z.H. Information extraction of sandy land. *Sci. Silvae Sin.* **2005**, *41*, 82–87.
75. Gao, Y.P.; Kang, M.D.; He, M.Z. Extraction of desert vegetation coverage based on visible light band information of unmanned aerial vehicle: A case study of Shapotou region. *J. Lanzhou Univ. Sci. Ed.* **2018**, *54*, 770–775.
76. Tang, L.; He, M.Z.; Li, X.R. Verification of Fractional Vegetation Coverage and NDVI of Desert Vegetation via UAVRS Technology. *Remote Sens.* **2020**, *12*, 1742. [[CrossRef](#)]
77. Aguiar, M.R.; Sala, O.E. Patch structure, dynamics and implications for the functioning of arid ecosystems. *Trends Ecol. Evol.* **1999**, *14*, 273–277. [[CrossRef](#)] [[PubMed](#)]
78. Okin, G.S. Connectivity in dryland landscapes: Shifting concepts of spatial interactions. *Front. Ecol. Environ.* **2016**, *13*, 20–27. [[CrossRef](#)] [[PubMed](#)]
79. Su, L.H. Support vector machines for recognition of semi-arid vegetation types using MISR multi-angle imagery. *Remote Sens. Environ.* **2007**, *107*, 299–311. [[CrossRef](#)]
80. Ding, J.; Li, Z.P.; Zhang, H.Y.; Zhang, P.; Cao, X.M. Quantifying the Aboveground Biomass (AGB) of Gobi Desert Shrub Communities in Northwestern China Based on Unmanned Aerial Vehicle (UAV) RGB Images. *Land* **2022**, *11*, 543. [[CrossRef](#)]
81. Diallo, H.A. United Nations Convention to Combat Desertification. In *The Future of Drylands*; Springer: Dordrecht, The Netherlands, 2008; pp. 104–113.
82. Briassoulis, H. Combating Land DEgradation and Desertification: The Land-Use Planning Quandary. *Land* **2019**, *8*, 27. [[CrossRef](#)]
83. Wang, T.; Song, X.; Yan, C.Z. The trend of desertification in northern China in the past 35 years Remote Sensing Analysis. *J. Desert Res.* **2011**, *31*, 1351–1356.
84. Wang, T. *Atlas of Deserts and Desertification in Northern China*; Science Press: Beijing, China, 2014.
85. Al-Dabi, H.; Koch, M.; Al-Sarawi, M.; El-Baz, F. Evolution of sand dune patterns in space and time in north-western Kuwait using Landsat images. *J. Arid Environ.* **1997**, *36*, 15–24. [[CrossRef](#)]
86. Yao, Z.Y.; Wang, T.; Han, Z.W.; Zhang, W.M.; Zhao, A.G. Migration of sand dunes on the northern Alxa Plateau, Inner Mongolia. China. *J. Arid Environ.* **2007**, *70*, 80–93. [[CrossRef](#)]
87. Bandeira, L.; Marques, J.S.; Saraiva, J.; Pina, P. Automated detection of Martian dune fields. *IEEE Geosc. Remote Sens.* **2011**, *8*, 626–630.
88. Azzaoui, M.A.; Adnani, M.; Belhiti, H.; Chaouki, I.E.; Masmoudi, C. Detection of barchan dunes in high resolution satellite images. *Int. Arch. Photogramm.* **2016**, *41*, 153–163.
89. Weng, L.; Wang, L.; Xia, M.; Shen, H.; Liu, J.; Xu, Y. Desert classification based on a multi-scale residual network with an attention mechanism. *Geosci. J.* **2020**, *25*, 387–399. [[CrossRef](#)]
90. Xia, M.; Tian, N.; Zhang, Y.; Xu, Y.; Zhang, X. Dilated multi-scale cascade forest for satellite image classification. *Remote Sens.* **2020**, *41*, 7779–7800. [[CrossRef](#)]
91. Ge, G.; Shi, Z.; Zhu, Y.; Yang, X.; Hao, Y. Land Use/Cover Classification in an Arid Desert-Oasis Mosaic Landscape of China Using Remote Sensed Imagery: Performance Assessment of Four Machine Learning Algorithms. *Glob. Ecol. Conserv.* **2020**, *22*, e00971. [[CrossRef](#)]
92. Du, H.S.; Wang, J.F.; Han, C. High-precision remote sensing mapping of aeolian sand landforms based on deep learning algorithms. *Open Geosci.* **2022**, *14*, 224–233. [[CrossRef](#)]
93. Aydda, A.; Althuwaynee, O.F.; Pokharel, B. An easy method for barchan dunes automatic extraction from multispectral satellite data. *IOP Conf. Ser. Earth Environ. Sci.* **2020**, *419*, 012015. [[CrossRef](#)]
94. Liu, X.; Pei, F.; Wen, Y.; Li, X.; Wang, S. Global Urban Expansion Offsets Climate-Driven Increases in Terrestrial Net Primary Productivity. *Nat. Commun.* **2019**, *10*, 5558. [[CrossRef](#)] [[PubMed](#)]
95. Liu, Y.H.; Dong, Y.X. Tentative Study on Desertification and Sustainable Development in China. *J. Desert Res.* **1999**, *19*, 17–22.
96. Lei, Y.H.; Ding, G.D.; Li, Z.M.; Chi, W.F.; Gao, G.L. Land Use/cover Change and its Ecosystem Service Value Response in the Beijing-Tianjin Sandstorm Source Control Project Area. *J. Desert Res.* **2021**, *41*, 29–40.
97. Lin, L.Z.; Chen, Y.S.; Ma, W.Z.; Lin, Z.; Yu, Q. Evolution and Driving Forces of Ecosystem Pattern in Kubuqi Desert of Northern China. *J. Beijing For. Univ.* **2021**, *43*, 108–123.
98. Zhan, Q.; Zhao, W.; Yang, M.; Xiong, D. A Long-Term Record (1995–2019) of the Dynamics of Land Desertification in the Middle Reaches of Yarlung Zangbo River Basin Derived from Landsat Data. *Geogr. Sustain.* **2021**, *2*, 12–21. [[CrossRef](#)]
99. Zhang, Z.; Wang, X.; Zhao, X.; Liu, B.; Yi, L. A 2010 Update of National Land Use/Cover Database of China at 1:100000 Scale Using Medium Spatial Resolution Satellite Images. *Remote Sens. Environ.* **2014**, *149*, 142–154. [[CrossRef](#)]
100. Piao, S.; Fang, J.; Ji, W.; Guo, Q.; Ke, J. Variation in a Satellite-Based Vegetation Index in Relation to Climate in China. *J. Veg. Sci.* **2004**, *15*, 219–226. [[CrossRef](#)]
101. Feng, X.; Fu, B.; Piao, S.; Wang, S.; Ciais, P. Revegetation in China's Loess Plateau Is Approaching Sustainable Water Resource Limits. *Nat. Clim. Chang.* **2016**, *6*, 1019–1022. [[CrossRef](#)]

102. Zolch, T.; Wamsler, C.; Pauleit, S. Integrating the Ecosystem-Based Approach into Municipal Climate Adaptation Strategies: The Case of Germany. *J. Clean. Prod.* **2018**, *170*, 966–977. [[CrossRef](#)]
103. Jiang, C.L.; Wu, L.; Liu, D.; Wang, S.M. Remote sensing dynamic monitoring of eco-environmental quality in arid desert areas: Taking the Gurbantunggut Desert as an example. *Chin. J. Appl. Ecol.* **2019**, *30*, 877–883.
104. Rouse, J.W.; Haas, R.H.; Schell, J.A. *Monitoring Vegetation Systems in the Great Plains with ERTS*; NASA: Washington, DA, USA, 1974; pp. 310–317.
105. Jiang, Z.Y.; Huete, A.R.; Didan, K.; Miura, T. Development of a two-band enhanced vegetation index without a blue band. *Remote Sens. Environ.* **2008**, *112*, 3833–3845. [[CrossRef](#)]
106. Li, B.L.; Zhou, C.H. Sandy desertification in the western sandy land of Northeast Plain in recent 10 years. *Acta Geogr. Sin.* **2001**, *56*, 307–315.
107. Ying, L.; Qian, J.X.; Hui, Y. Comprehensive Evaluation of Sentinel - 2 Red Edge and Shortwave-Infrared Bands to Estimate Soil Moisture. *IEEE J. Sel. Top. Appl. Earth Obs. Remote Sens.* **2021**, *14*, 7448–7465.
108. Wei, H.S.; Wang, J.L.; Han, B.M. Desertification Information Extraction along the China-Mongolia Railway Supported by Multi-Source Feature Space and Geographical Zoning Modeling. *IEEE J. Sel. Top. Appl. Earth Obs. Remote Sens.* **2020**, *13*, 392–402. [[CrossRef](#)]
109. Gitelson, A.A.; Stark, R.; Grits, U.; Rundquist, D.; Kaufman, Y.; Derry, D. Vegetation and soil lines in visible spectral space: A concept and technique for remote estimation of vegetation fraction. *Int. J. Remote Sens.* **2002**, *23*, 2537–2562. [[CrossRef](#)]
110. Xu, H.Q. A new index for delineating built-up land features in satellite imagery. *Int. J. Remote Sens.* **2008**, *29*, 4269–4276. [[CrossRef](#)]
111. Chen, W.H.; Liu, L.Y.; Zhang, C. Monitoring the seasonal bare soil areas in Beijing using multi-temporal TM images. *IEEE Int. Geosci. Remote Sens. Symp.* **2004**, *5*, 3379–3382.
112. Liu, Y.; Meng, Q.Y.; Zhang, L.L.; Wu, C.Y. NDBSI: A normalized difference bare soil index for remote sensing to improve bare soil mapping accuracy in urban and rural areas. *CATENA* **2022**, *214*, 106265. [[CrossRef](#)]
113. Meng, X.Y.; Gao, X.; Li, S.; Li, S.Y.; Lei, J.Q. Monitoring desertification in Mongolia based on Landsat images and Google Earth Engine from 1990 to 2020. *Ecol. Indic.* **2021**, *129*, 107908. [[CrossRef](#)]
114. Li, P.X.; Chen, P.; Shen, J.Q.; Deng, W.N.; Kang, X.L. Dynamic Monitoring of Desertification in Ningdong Based on Landsat Images and Machine Learning. *Sustainability* **2022**, *14*, 7470. [[CrossRef](#)]
115. Bezerra, F.G.S.; Aguiar, A.P.D.; Alvalá, R.C.S.; Girolla, A.; Bezerra, K.R.A.; Lima, P.V.P.S. Analysis of areas undergoing desertification, using EVI2 multi-temporal data based on MODIS imagery as indicator. *Ecol. Indic.* **2020**, *117*, 106579. [[CrossRef](#)]
116. Guo, B.; Ye, W. An Optimal Monitoring Model of Desertification in Naiman Banner Based on Feature Space Utilizing Landsat8 OLI Image. *IEEE Access* **2020**, *8*, 4761–4768. [[CrossRef](#)]
117. Liu, Q.; Liu, G.; Huang, C. Monitoring desertification processes in Mongolian Plateau using MODIS tasseled cap transformation and TGSi time series. *J. Arid Land* **2018**, *10*, 12–26. [[CrossRef](#)]
118. Liu, Y.; Dang, C.Y.; Yue, H. Comparison between modified remote sensing ecological index and RSEI. *Natl. Remote Sens. Bull.* **2022**, *26*, 683–697. [[CrossRef](#)]
119. Jiang, L.L.; Jiapaer, G.L.; Bao, A.M. Monitoring the long-term desertification process and assessing the relative roles of its drivers in Central Asia. *Ecol. Indic.* **2019**, *104*, 195–208. [[CrossRef](#)]
120. Zhang, T.; Yang, R.Q.; Yang, Y.B.; Li, L.; Chen, L.Q. Sensing Ecological Index: Application to Tianjin, North China. *ISPRS Int. J. Geo-Inf.* **2021**, *10*, 475. [[CrossRef](#)]
121. Hamada, Y.; Szoldatits, K.; Grippo, M.; Hartmann, H.M. Remotely Sensed Spatial Structure as an Indicator of Internal Changes of Vegetation Communities in Desert Landscapes. *Remote Sens* **2019**, *11*, 1495. [[CrossRef](#)]
122. Qin, Z.; Berliner, P.; Karnieli, A. Micrometeorological modeling to understand the thermal anomaly in the sand dunes across the Israel-Egypt border. *J. Arid Environ.* **2002**, *51*, 281–318. [[CrossRef](#)]
123. Feng, H.; Liu, H.; Wu, L. Monitoring the relationship between the land surface temperature change and urban growth in Beijing, China. *IEEE J. Sel. Top. Appl. Earth Obs. Remote Sens.* **2014**, *7*, 4010–4019. [[CrossRef](#)]
124. Feng, H.; Zou, B.; Luo, J. Coverage-dependent amplifiers of vegetation change on global water cycle dynamics. *J. Hydrol.* **2017**, *500*, 220–229. [[CrossRef](#)]
125. Yang, Y.; Cao, C.; Pan, X.; Li, X.; Zhu, X. Downscaling Land Surface Temperature in an Arid Area by Using Multiple Remote Sensing Indices with Random Forest Regression. *Remote Sens.* **2017**, *9*, 789. [[CrossRef](#)]
126. Pan, X.; Zhu, X.; Yang, Y.B.; Cao, C.; Zhang, X.Z. Applicability of Downscaling Land Surface Temperature by Using Normalized Difference Sand Index. *Sci. Rep.* **2018**, *8*, 9530. [[CrossRef](#)] [[PubMed](#)]
127. Jiang, Z.; Ni, X.; Xing, M. A Study on Spatial and Temporal Dynamic Changes of Desertification in Northern China from 2000 to 2020. *Remote Sens.* **2023**, *15*, 1368. [[CrossRef](#)]
128. Feng, K.; Wang, T.; Liu, S.L.; Kang, W.P.; Chen, X. Monitoring Desertification Using Machine-Learning Techniques with Multiple Indicators Derived from MODIS Images in Mu Us Sandy Land, China. *Remote Sens.* **2022**, *14*, 2663. [[CrossRef](#)]
129. Elbeih, S.F. Evaluation of agricultural expansion areas in the Egyptian deserts: A review using remote sensing and GIS. *Egypt. J. Remote Sens. Space Sci.* **2021**, *24*, 889–906. [[CrossRef](#)]
130. Xu, D.; You, X.; Xia, C. Assessing the spatial-temporal pattern and evolution of areas sensitive to land desertification in North China. *Ecol. Indic.* **2019**, *97*, 150–158. [[CrossRef](#)]

131. Lehmkuhl, F.; Nett, J.J.; Poetter, S.; Schulte, P.; Sprafke, T. Loess landscapes of Europe-Mapping, geomorphology, and zonal differentiation. *Earth-Sci. Rev.* **2021**, *215*, 103496. [[CrossRef](#)]
132. Ali, K.; Johnson, B.A. Land-Use and Land-Cover Classification in Semi-Arid Areas from Medium-Resolution Remote Sensing Imagery: A Deep Learning Approach. *Sensors* **2022**, *22*, 8750. [[CrossRef](#)]
133. Dang, X.; Na, Y.; Chi, W.F.; Zhao, J.J. Spatio-Temporal Evolution of Sandy Land and its Impact on Soil Wind Erosion in the Kubuqi Desert in Recent 30 Years. *Front. Environ. Sci.* **2022**, *10*, 950196. [[CrossRef](#)]
134. Yu, J.; Wu, H.Q.; Fan, Y.M.; Gu, J.Z.; Shi, M.J. Research on Boundary Extraction of Kumtag Desert Based on Remote Sensing Technology. *Agric. Sci.-Technol. Inf.* **2021**, *23*, 19–21+24.
135. Tian, D.Y.; Zhang, Y.N.; Zhao, G.H. Convolutional Neural Network for Remote Sensing Plant Cover Extracting. *Remote Sens. Technol. Appl.* **2018**, *33*, 151–157.
136. Wang, L.X. Desert Remote Sensing Image Recognition Based on Multi-Resolution Feature Fusion. Master's Thesis, Nanjing University of Information Technology, Nanjing, China, 2021.
137. Zhang, Z.Y.; Cao, W.H.; Zhu, R.; Hu, W.K.; Wu, M. Scene classification method of high resolution remote sensing image based on sparse representation of spiking convolutional neural network. *Control Decis.* **2022**, *37*, 2305–2313.
138. Yann, L.c.; Bengio, Y.; Hinton, G. Deep learning. *Nature* **2015**, *521*, 436–444.
139. Krizhevsky, A.; Sutskever, I.; Hinton, G.E. Imagenet classification with deep convolutional neural networks. *Adv. Neural Inf. Process. Syst.* **2012**, *1*, 1097–1105. [[CrossRef](#)]
140. Long, J.; Shelhamer, E.; Darrell, T. Fully Convolutional Networks for Semantic Segmentation. *IEEE Trans. Pattern Anal. Mach. Intell.* **2015**, *39*, 640–651.
141. He, K.; Zhang, X.; Ren, S. Deep residual learning for image recognition. In Proceedings of the IEEE Conference on Computer Vision And Pattern Recognition, Las Vegas, NV, USA, 27–30 June 2016.
142. Geng, J.; Fan, J.; Wang, H. High-Resolution SAR Image Classification via Deep Convolutional Autoencoders. *IEEE Geosci. Remote Sens. Lett.* **2015**, *12*, 1–5. [[CrossRef](#)]
143. Chen, Y.; Zhao, X.; Jia, X. Spectral-Spatial Classification of Hyperspectral Data Based on Deep Belief Network. *IEEE J. Sel. Top. Appl. Earth Obs. Remote Sens.* **2015**, *8*, 2381–2392. [[CrossRef](#)]
144. Liang, H.M.; Li, Q. Hyperspectral Imagery Classification Using Sparse Representations of Convolutional Neural Network Features. *Remote Sens.* **2016**, *8*, 99. [[CrossRef](#)]
145. Hu, W.; Huang, Y.Y.; Wei, L. Deep Convolutional Neural Networks for Hyperspectral Image Classification. *J. Sens.* **2015**, *2015*, 258619. [[CrossRef](#)]
146. Liu, D.w.; Han, L.; Han, X.y. High spatial resolution remote sensing image classification based on deep learning. *Acta Opt. Sin.* **2016**, *36*, 0428001.
147. Yang, J.S.; Mei, T.C.; Zhong, S.D. Application of CNN, which takes care of local characteristics in the remote sensing image classification. *Comput. Eng. Appl.* **2018**, *54*, 188–195.
148. Gao, C.X.; Sang, N. Deep learning for object detection in remote sensing image. *Bull. Surv. Mapp.* **2014**, *1*, 108–111.
149. Zhao, W.; Du, S.; Emery, W.J. Object-Based Convolutional Neural Network for High-Resolution Imagery Classification. *IEEE J. Sel. Top. Appl. Earth Obs. Remote Sens.* **2017**, *10*, 3386–3396. [[CrossRef](#)]
150. Anthonsen, K.L.; Clemmensen, L.B.; Jensen, J.H. Volution of a dune from crescentic to parabolic form in response to short-term climatic changes: Råbjerg Mile, Skagen Odde, Denmark. *Geomorphology* **1996**, *17*, 63–77. [[CrossRef](#)]
151. Necsoiu, M.; Sébastien, L.; Hooper, D.M. Monitoring migration rates of an active subarctic dune field using optical imagery. *Remote Sens. Environ.* **2009**, *113*, 2441–2447. [[CrossRef](#)]
152. Brown, D.G.; Arbogast, A.F. Digital photogrammetric change analysis as applied to active coastal dunes in Michigan. *Photogramm. Eng. Remote Sens.* **1999**, *65*, 467–474.
153. Lyons, M.B.; Mills, C.H.; Gordon, C.E.; Letnic, M. Linking trophic cascades to changes in desert dune geomorphology using high-resolution drone data. *J. R. Soc. Interface* **2018**, *15*, 20180327. [[CrossRef](#)] [[PubMed](#)]
154. Zhao, X.M. Research on Information Extraction of Sand Dune Type Based on Deep Learning. Master's Thesis, Xinjiang University, Urumqi, China, 2021.
155. Elbelrhiti, H.; Claudin, P.; Andreotti, B. Field evidence for surface-wave-induced instability of sand dunes. *Nature* **2005**, *437*, 720–723. [[CrossRef](#)] [[PubMed](#)]
156. Chang, Z.F. Stability mechanisms of barchan dunes: A case study of Hexi Desert area in Gansu Province. *Earth Environ. Sci.* **2017**, *82*, 26–29. [[CrossRef](#)]
157. Jia, G.P.; Yang, G.; Han, X.Y.; Zuo, H.J.; Yao, Y.F. Quantitative Study on Morphological Characteristics of Barchan Dunes in Yamarak Desert, China. *Front. Earth Sci.* **2022**, *10*, 861991.
158. Pye, K.; Tsoar, H. *Aeolian Sand and Sand Dunes*; Springer: Berlin/Heidelberg, Germany, 2009; pp. 25–35.
159. Wasson, R.J.; Hyde, R. Factors determining desert dune type. *Nature* **1983**, *304*, 337–339. [[CrossRef](#)]
160. Hunter, R.E.; Richmond, B.M.; Alpha, T.R. Storm-controlled oblique dunes of the Oregon Coast. *Geol. Soc. Am. Bull.* **1983**, *94*, 1450–1465. [[CrossRef](#)]
161. Rubin, D.M.; Hunter, R.E. Bedform alignment in directionally varying flows. *Science* **1987**, *237*, 276–278. [[CrossRef](#)]
162. Julez, B. A Method of Coding TV Signals Based on Edge Detection. *Bell Syst. Tech. J.* **1959**, *4*, 1001–1020. [[CrossRef](#)]

163. Roberts, L.G. Mathine Perception of Three-Dimension Solids. In *Optimal and Electro-Optimal Information Processing*; MIT Press: Cambridge, MA, USA, 1965; pp. 99–197.
164. Prewitt, J.M.S. Object Enhancement and Extraction. In *Picture Processing and Psychopictorics*; Academic Press: Cambridge, MA, USA, 1970.
165. Dong, H.Y. Research on Several Techniques of Edge Detection. Ph.D. Thesis, National University of Defense Technology, Changsha, China, 2008.
166. Canny, J. A computational approach to edge detection. *Pattern Anal. Mach. Intell.* **1986**, *8*, 679–698. [[CrossRef](#)]
167. Xu, L.; Wei, R. Image Edge Detection Optimization Algorithm Based on Canny Operator. *Sci. Technol. Bull.* **2013**, *29*, 127–131.
168. Han, L.L.; Tian, Y.M.; Qi, Q.H. Research on edge detection algorithm based on improved Sobel operator. *MATEC Web Conf.* **2020**, *309*, 03031. [[CrossRef](#)]
169. Lee, J.; Haralick, R.; Shapiro, L. Morphologic edge detection. *IEEE J. Robot. Autom.* **1987**, *3*, 142–156. [[CrossRef](#)]
170. Kumar, M.; Singh, S. Edge Detection And Denoising Medical Image Using Morphology. *Int. J. Eng. Sci. Emerging Technol.* **2012**, *2*, 66–72.
171. Ge, A.L. Improved adaptive morphological edge detection method. *J. Ningxia Univ. Nat. Sci. Ed.* **2016**, *37*, 5.
172. Huang, H.L.; Wang, H. An Edge Detection Algorithm Based on Wavelet Transform and Mathematical Morphology. *J. Northeast. Univ.* **2011**, *32*, 1315–1318.
173. Zhang, Z.G.; Zheng, X.; Lan, J.C. Image Edge Detection Based on Interpolation Wavelet Tower Decomposition Algorithm. *Comput. Sci.* **2017**, *44*, 164–168.
174. Jiang, C.W.; Dong, Z.B.; Wen, Q. Extraction of Dune Crest Lines and Calculation of Dune-field Pattern Parameters on Remote Sensing Image Based on MATLAB Platform. *J. Desert Res.* **2013**, *33*, 1636–1642.
175. Gao, B.Y.; Yang, B.; Zhang, D.G. Extracting the sand dune crest lines from satellite images using U-Net deep convolutional neural network. *J. Desert Res.* **2021**, *41*, 21–32.

Disclaimer/Publisher’s Note: The statements, opinions and data contained in all publications are solely those of the individual author(s) and contributor(s) and not of MDPI and/or the editor(s). MDPI and/or the editor(s) disclaim responsibility for any injury to people or property resulting from any ideas, methods, instructions or products referred to in the content.